Geophysical Journal International

Geophys. J. Int. (2014) **198,** 366–384
Advance Access publication 2014 May 20
GJI Geodynamics and tectonics

doi: 10.1093/gji/ggu142

High-resolution Quaternary and Neogene reconstructions of Eurasia-North America plate motion

S. Merkouriev[1] and C. DeMets[2]

[1] *Pushkov Institute of Terrestrial Magnetism of the Russian Academy of Sciences, St Petersburg Filial.* 1 *Mendeleevskaya Liniya, St Petersburg* 199034, *Russia. E-mail: chuck@geology.wisc.edu*
[2] *Department of Geoscience, University of Wisconsin-Madison, Madison, WI* 53706*, USA*

Accepted 2014 April 11. Received 2014 April 10; in original form 2014 January 28

SUMMARY

We estimate Eurasia-North America plate motion rotations at ∼1-Myr intervals for the past 20 Myr from more than 11 000 crossings of 21 magnetic reversals from Chron 1n (0.78 Ma) to C6no (19.72 Ma) and flow lines digitized from the Charlie Gibbs, Bight and Molloy fracture zones and transform faults. Adjusted for outward displacement, the 21 best-fitting rotations determined from a simultaneous inversion of the numerous kinematic data reconstruct the reversal crossings with weighted root mean square misfits of only 1–2 km and 0.2–7 km for the transform fault and fracture zone crossings. The new rotations clearly define a ∼1000 km southward shift of the rotation pole and 20 per cent slowdown in seafloor spreading rates between 7 and 6 Ma, preceded by apparently steady plate motion from 19.7 to ∼7 Ma. Data for times since C3An.2 (6.7 Ma) are well fit by a stationary pole of rotation and constant rate of angular opening, consistent with steady motion since 6.7 Ma. The southward shift of the rotation pole at 7–6 Ma implies that Eurasia-North America motion in northeastern Asia changed from slowly convergent before 7 Ma to slowly divergent afterward. Crossings of magnetic reversals C1n through C3An.1 (6.0 Ma) are well fit everywhere in the Arctic basin and south to the Azores triple junction, indicating that the Eurasia and North America plates have not deformed along their mutual boundary since at least 6.0 Ma. However, the new rotations systematically overrotate magnetic lineations older than C3An.1 (6.0 Ma) within 200 km of the Azores triple junction and also overrotate lineations older than C5n along the Gakkel Ridge in the Arctic Basin. Barring misidentifications of the magnetic anomalies in those areas, the pattern and magnitude of the systematic misfits imply that slow (∼1 mm yr^{-1}) distributed or microplate deformation occurred in one or both regions.

Key words: Plate motions; Arctic region; Atlantic Ocean.

1 INTRODUCTION

Accurate estimates of the Cenozoic relative motions of the Eurasia and North America plates have long been a focus of plate kinematic research, both to better understand the tectonic history of their 8000-km-long boundary in the north Atlantic and Arctic (Fig. 1) and determine the interactions of Eurasia and North America with the 13 other tectonic plates that border them. Over the past decade, two studies have documented in significant detail Eurasia-North America relative motion since 80 Ma. Gaina *et al.* (2002) estimate best-fitting finite rotations at ≈10 Myr intervals since 80 Ma from magnetic reversal crossings extracted from the Arctic and North Atlantic magnetic anomaly grid (Macnab *et al.* 1995; Verhoef *et al.* 1996) and fracture zone crossings extracted from the marine gravity grid of Sandwell & Smith (1997). At higher temporal resolution, Merkouriev & DeMets (2008) estimate finite rotations at ≈1 Myr intervals spanning the Quaternary and much of the Neogene from magnetic reversals they identified from dense surveys of the Kolbeinsey, Iceland, and northern Mid-Atlantic ridges (Fig. 2). Encouragingly, the opening distances that are predicted by the C5 and C6 rotations from these independent studies agree to within 1 per cent (Merkouriev & DeMets 2008), suggesting that the relative positions of the two plates can be reconstructed to within several kilometres over periods spanning tens of millions of years.

Here, we update our previous analysis (Merkouriev & DeMets 2008, hereafter abbreviated MD08), with two principal motivations. The increasing geopolitical importance of the Arctic Basin calls for reconstructions of the basin's natural history that are grounded in the best-available data. Given that none of the magnetic data used by MD08 are from the Arctic basin seafloor spreading centres, we elected to update our earlier analysis using high-quality magnetic survey data for the Mohns and Gakkel ridges in the far Arctic (Fig. 2). The additional data not only reduce the noise and uncertainties in the estimated rotations, but permit us to test for data

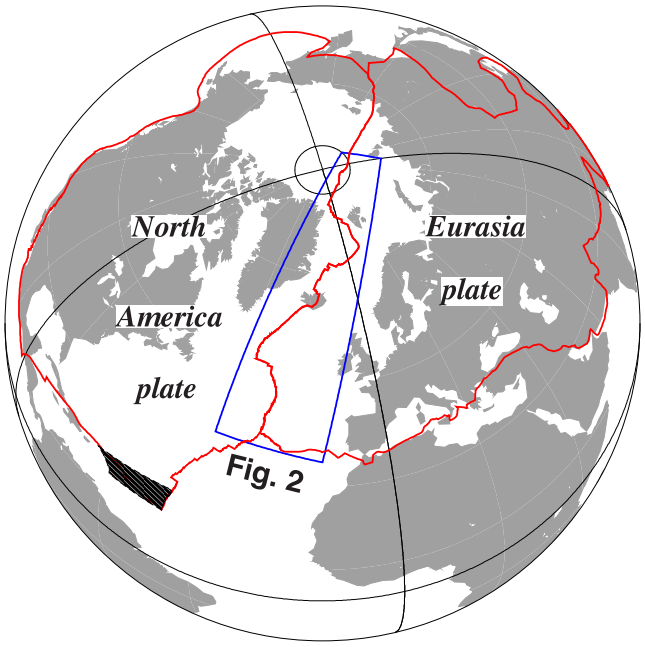

Figure 1. Study area location map. Red lines show Eurasia and North America plate boundaries. Blue lines show the limits of the map in Fig. 2, which encloses the region from which the marine magnetic and bathymetric data used for the analysis is taken.

biases and/or deformation along the whole plate boundary during much of the Neogene. Our second motivation is to update our rotation estimates using an improved method for fitting observations of magnetic reversals, fracture zones and transform faults, as described by Merkouriev & DeMets (2014). Our analysis thus incorporates kinematic information from the Charlie Gibbs, Bight and Molloy fracture zones and transform faults not used by MD08.

2 DATA

Two types of data are used here to estimate plate rotations. Ship and airplane magnetic surveys of the Mid-Atlantic Ridge, Reykjanes Ridge and Arctic Basin spreading centres (Fig. 2) are used to identify crossings of magnetic polarity reversals C1n through C6no (Table 1 and Fig. 3). Bathymetric grids from the Marine Geoscience Data System (www.marine-geo.org and Carbotte *et al.* 2004) are used to define fracture zone flow lines and transform faults, which constrain palaeo- and present-day plate slip directions, respectively. Details are given below.

2.1 Magnetic reversal crossings

Fig. 2 shows the ship and airplane track lines of all the magnetic data used for our present analysis and by MD08. From magnetic surveys of the Kolbeinsey Ridge, Reykjanes Ridge and the Mid-Atlantic Ridge between the Azores triple junction and ≈50°N, we previously identified 7150 magnetic reversal crossings of chrons 1n through 6n. The remarkably clear and complete magnetic anomaly sequences from the slow-spreading Reykjanes and Kolbeinsey ridges strongly constrain the Quaternary and Neogene histories of Eurasia-North America motion (MD08) and remain the foundation of this analysis.

To complement these observations, we made additional reversal identifications from surveys of the ultraslow-spreading Mohns and

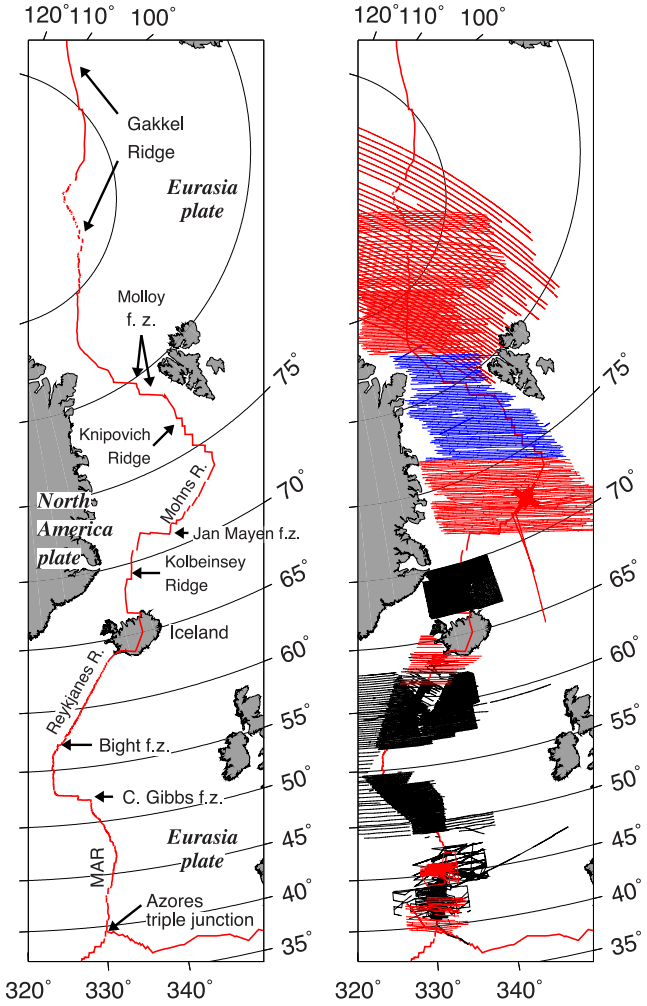

Figure 2. Left—Locations of features described in text. Red lines mark plate boundaries within the study area. Abbreviations: f.z., fracture zone; R., ridge; MAR, Mid-Atlantic Ridge. Right—Black lines show magnetic survey lines used here and by Merkouriev & DeMets (2008). Red lines indicate data used in this study, but not by Merkouriev & DeMets (2008). Blue lines show Knipovich Ridge aeromagnetic survey for which magnetic anomaly sequences were not successfully identified. Both maps are oblique Mercator projections about the rotation pole for C5n.2.

Gakkel Ridges in the Arctic Basin, the northernmost Reykjanes Ridge and the Mid-Atlantic Ridge north of the Azores triple junction (shown by the red lines in Fig. 2). Our sources of data in the Arctic Basin are U.S. Naval Research Laboratory aeromagnetic surveys from the 1970s and late 1990s of the Mohns, Knipovich and Gakkel ridges (Fig. 2; Feden *et al.* 1979; Vogt *et al.* 1979; Kovacs *et al.* 1982), and a dense shipboard survey of the Mohns Ridge at 72–73°N (Géli *et al.* 1994). We also use newly available, well-navigated shipboard profiles from the R/V Knorr 189 survey of the northern end of the Reykjanes Ridge (Hey *et al.* 2010; Benediktsdóttir *et al.* 2012) and magnetic data from the Mid-Atlantic Ridge between the Azores triple junction and ≈50°N.

From these data, we identified crossings of 21 magnetic polarity reversals (listed in Table 1 and displayed in Fig. 3), ranging in age from 0.781 Ma (the old edge of Anomaly 1n) to 19.7 Ma (the old edge of Anomaly 6). The 21 correlation points coincide with either the young or old edge of a magnetic polarity interval (Fig. 3) and are the same as those used by MD08. Reversal ages,

Table 1. Data summary.

Magnetic	Age	Number of data			wrms misfits (km)		
reversal	(Ma)	Anom	FZ	TF	Anom	FZ	TF
1no	0.781	734	92	313	1.11	0.24	0.36
2ny	1.778	962	79	–	1.16	0.51	–
2An.1y	2.581	1102	70	–	1.22	0.81	–
2An.3o	3.596	946	79	–	1.47	1.03	–
3n.1y	4.187	660	34	–	1.46	1.37	–
3n.4o	5.235	691	68	–	1.34	1.42	–
3An.1y	6.033	651	34	–	1.23	1.81	–
3An.2o	6.733	585	44	–	1.40	1.87	–
4n.1y	7.528	576	47	–	1.52	1.57	–
4n.2o	8.108	635	39	–	1.44	1.48	–
4Ao	9.105	453	59	–	1.33	1.81	–
5n.1y	9.786	606	53	–	1.83	2.05	–
5n.2o	11.056	679	68	–	1.80	2.09	–
5An.2o	12.474	359	96	–	1.84	1.96	–
5ACy	13.739	225	70	–	1.79	1.70	–
5ADo	14.609	210	51	–	1.81	1.97	–
5Cn.1y	15.974	297	95	–	1.86	2.59	–
5Dy	17.235	257	59	–	2.11	2.92	–
5Ey	18.056	297	56	–	1.81	4.08	–
6ny	18.748	321	45	–	2.01	6.56	–
6no	19.722	308	139	–	1.78	6.97	–

Notes: Chron designators followed by a 'y' or 'o', respectively indicate the young or old edge of the chron. All but one of the reversal ages, that for C4n.1y, are from the astronomically-tuned Neogene timescale of Hilgen *et al.* (2012; also see Ogg 2012). The age for C4n.1y is not specified by Hilgen *et al.* (2012). We instead adopt its age from the astronomically tuned reversal timescale of Lourens *et al.* (2004), which is consistent with that of Hilgen *et al.* (2012) for all reversals younger than C4r.1n. 'Anom', 'FZ', and 'TF', respectively, indicate the number of magnetic anomaly, fracture zone, and transform fault crossings used to estimate the finite rotations in Tables 2 and 3. Although ages are not assigned to fracture zone crossings for the inversions, they are approximated afterwards from the age of the nearest point along the modelled fracture zone flow lines, 'wrms' is the weighted root-mean-square misfit in kilometres for the rotation that best fits the data for each reversal.

which are given in Table 1, are adopted from the astronomically tuned geomagnetic reversal timescale GTS2012 (Hilgen *et al.* 2012; Ogg 2012).

Along the Reykjanes Ridge, where magma production rates are high due to the proximity of the Iceland hotspot, the magnetic anomalies are well defined and easily correlated with a synthetic magnetic profile (Fig. 3). In contrast, magnetic anomaly sequences from the Mohns and Gakkel ridges lack the shorter-duration anomalies seen along the Reykjanes ridge and are harder to correlate (Fig. 3), presumably due to a combination of slower spreading rates (10–15 mm yr^{-1}) and fault-dominated, amagmatic extension in some areas (Michael *et al.* 2003). Despite the lower fidelity of the Arctic Basin magnetic lineations, we successfully identified all magnetic reversals younger than C5An.2 along the Mohns and Gakkel ridges. We were less successful at identifying some of the anomalies older than C5An.2. For example, Anomaly 6 was the only anomaly older than C5An.2 that we could identify with any confidence along the Gakkel Ridge. Along the Mohns Ridge, we were unable to distinguish the short-duration anomalies C5AC and C5AD from the other reversals within the 5AA-5B anomaly sequence. As documented in Section 4.2.2, we attribute larger average misfits for the Arctic Basin reversal crossings, particularly for anomalies older than C5An.2, to the lower resolution of the Arctic Basin magnetic anomalies.

We were unable to identify with high confidence any of the magnetic anomalies along the well-surveyed, but highly-segmented and obliquely spreading Knipovich Ridge (Fig. 2). Consequently, none of the Knipovich Ridge data are used for the analysis.

Overall, we identified more than 12 000 crossings of magnetic reversals C1n to C6n. Of these, 11 554 are used to estimate the Eurasia-North America rotations described below (Fig. 4). The remaining ∼600 reversal crossings are located in areas of possible microplate deformation (described below) and were used in only the first stage of our analysis. The number of magnetic reversal crossings that are used to estimate the Eurasia-North America plate rotations ranges from more than 1000 for C2An.1 to as few as 210 for C5AD (Table 1). All of the reversal crossings used to estimate the new Eurasia-North America rotations are included in the newly established, open-source reversal repository described by Seton *et al.* (2014).

2.2 Fracture zone flow lines and transform faults

Four well-defined fracture zones offset the Eurasia-North America plate boundary—the double-stranded Charlie Gibbs fracture zone (Searle 1981), the Molloy fracture zone (Crane *et al.* 2001), and the Bight and Jan Mayen fracture zones (Figs 2 and 4). We digitized the traces of all four from bathymetric grids extracted from the Marine Geoscience Data System (www.marine-geo.org and Carbotte *et al.* 2004). The digitized fracture zone crossings are spaced every 1.2 to 1.8 km, approximately the same as the resolution of the bathymetric grids from which the fracture zones were digitized.

We assigned uncertainties to each transform fault and fracture zone crossing as follows. We first identified any morphologic features within the fracture zone valley that clearly bound the zone of active faulting or palaeofaulting. We then measured the distance across the valley between those features. If no such features were apparent, we measured the width of the entire fracture zone valley. These cross-valley distances vary from as little as 2 km where multibeam or single-beam bathymetry clearly delineate the zone of active or palaeoshear to as much as 24 km where the zone of palaeoshear is only constrained to lie somewhere within the fracture zone valley. Finally, we equated the half-width of the cross-valley distances to the 95 per cent uncertainty in the location of the shear zone within the valley, thereby giving assigned 1-σ uncertainties (half of the 95 per cent uncertainty) of $\pm$0.5 to $\pm$6 km. Below, we show that the estimated uncertainties are ∼25 per cent larger and hence more conservative than warranted by the model fits. We did not further adjust the fracture zone uncertainties for the analysis below.

3 METHODS

3.1 Estimation of finite rotations

In our previous study (MD08), we estimated best-fitting finite rotations using a minimum-distance, great-circle fitting criterion to reconstruct both the magnetic reversal and fracture zone crossings (Hellinger 1979; Chang 1988; Royer & Chang 1991). Here, we instead fit crossings of magnetic reversals, fracture zones and transform faults with separate fitting functions appropriate for each type of data (Merkouriev & DeMets 2014). Magnetic reversal crossings are reconstructed using the same great-circle fitting criterion described by Hellinger (1979, 1981). The digitized traces of strike-slip faults within transform fault valleys are fit as lines of pure slip

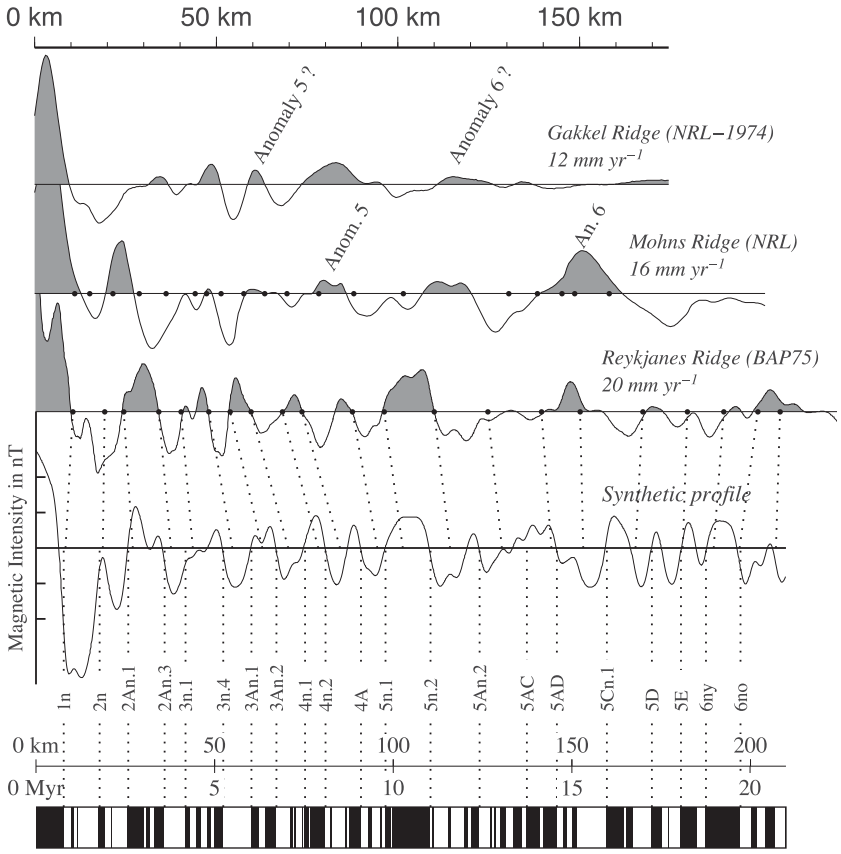

Figure 3. Comparison of observed magnetic anomaly profiles from the Gakkel, Mohns and Reykjanes ridges to synthetic magnetic profile created for a full spreading rate of 20 mm yr^{-1}, a 500-m wide reversal transition zone and ambient and palaeomagnetic inclinations and declinations appropriate for the Reykjanes Ridge. The magnetic block model and 21 reversal correlation points (dotted lines) used for this study appear below the synthetic magnetic anomaly profile. The three observed profiles approximate plate flow lines and sample spreading at rates that decrease from ≈20 mm yr^{-1} along the Reykjanes Ridge to 12 mm yr^{-1} along the Gakkel Ridge. The transition from slow, magma-dominated spreading along the Reykjanes Ridge to ultraslow, fault-dominated spreading along the Gakkel Ridge and corresponding loss in the fidelity of the magnetic reversal record makes reversal identifications along the Mohns and Gakkel ridges increasingly difficult.

(i.e. small circles) around the youngest pole of opening. Fracture zones are assumed to define flow lines that can be reconstructed with a time progression of stage rotations and hence finite rotations. We adopt the fracture zone fitting method described by Shaw & Cande (1990), whereby flow lines that originate at ridge-transform intersections on one or both sides of the ridge are constructed from stage rotations that are derived from a time-series of finite rotations whose values are adjusted iteratively to minimize the summed least-squares distance between the modelled flow lines and digitized fracture zone flow lines.

The best-fitting sequence of finite rotations is estimated from a single inversion of all the magnetic reversal, fracture zone and transform fault crossings (Merkouriev & DeMets 2014). Because the rotations for different times are correlated to varying degrees, information for well-determined rotations propagates into and improves rotation estimates for times for which fewer data are available. Conversely, problems such as incorrectly identified magnetic reversals or inaccurate fracture zone flow lines may propagate into and thus degrade estimates for multiple rotations.

As is described below, all of the plate motion rotations are also corrected for the biasing effect of outward displacement (Merkouriev & DeMets 2006, 2008, 2014).

We use stage rotations and their covariances, which are derived rigorously from the finite rotations and their covariances, to describe motion during 1–3 Myr intervals. We selected 1–3 Myr-long intervals in order to keep the 2-σ (95 per cent) stage rate uncertainties below ±1 mm yr^{-1} given the combined uncertainties in the stage rotations and magnetic reversal age dates. For magnetic reversals whose ages are astronomically calibrated, errors in their estimated ages are unlikely to exceed ±5000–10 000 yr (Lourens *et al.* 2004). The implied standard error in a stage spreading rate that averages motion over 1.5 Myr, the approximate length of the shortest averaging interval that we use, is only 0.6 per cent of the stage rate or about ±0.1 mm yr^{-1} for the 15–20 mm yr^{-1} full spreading rates that are typical of Eurasia-North America motion. Such errors are a factor of 2–10 smaller than the uncertainties propagated from the rotation covariances and thus do not represent an important limiting factor in our analysis. Although uncertainties in our estimates of outward displacement also affect each of our finite rotations, they do not significantly affect the stage rotations because any bias in the finite rotations due to incorrectly estimated outward displacement is common to all the finite rotations and is thus cancelled upon differencing those rotations to estimate stage rotations.

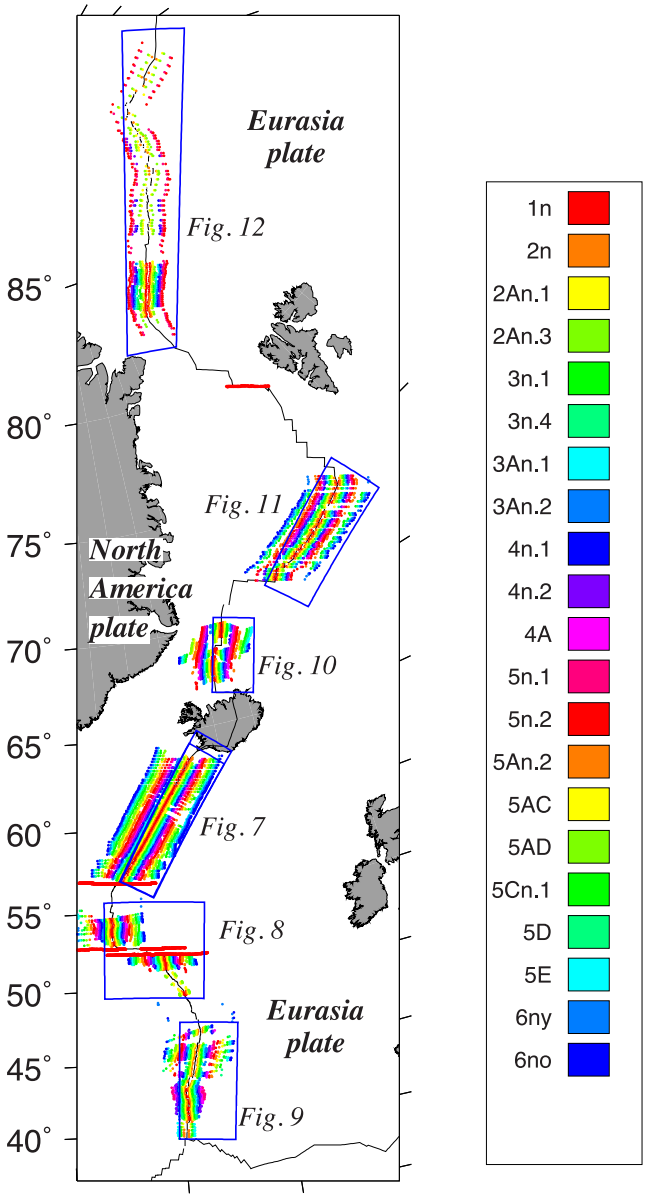

Figure 4. Locations of data used to estimate the best-fitting Eurasia-North America rotations in Table 2. Colour-coded circles show the locations of all 11 554 identifications of magnetic reversals C1no through C6no from the tracks shown in Fig. 2. The digitized fracture zone flow lines and transform faults (red circles) are shown in greater detail in Fig. 13. Areas outlined in blue show the locations of the plate reconstructions in Figs 7–12.

3.2 Data dispersion

Following Royer & Chang (1991), we use the parameter $\hat{\kappa} = (N - m)/\chi^2$ as a measure of the goodness-of-fit of the best-fitting rotations, where N is the number of observations, m is the number of parameters used to fit the data and χ^2 is the weighted least-squares misfit to the data. Values of $\hat{\kappa} \simeq 1$ indicate that the estimated data uncertainties are approximately correct, whereas values of $\hat{\kappa}$ that are significantly greater or less than 1 indicate that the uncertainties are, respectively, overestimated or underestimated. Rescaling of the data uncertainties by a factor of $\sqrt{\hat{\kappa}}$ can be used to adjust the data uncertainties and hence model uncertainties so that they better approximate the underlying data dispersion.

For a single time interval and palaeoplate boundary defined by data from P spreading segments, Q fracture zone flow lines and R transform faults, $\hat{\kappa}$ for each type of data is well approximated as follows: (1) $(N_{\rm mag} - 2P) / \chi^2{}_P$ for $N_{\rm mag}$ magnetic reversal crossings, (2) $N_{fz}/\chi^2{}_Q$ for N_{fz} fracture zone crossings, and (3) $(N_{tf} - R) / \chi^2{}_R$ for N_{tf} transform fault crossings.

3.3 Estimation of finite rotation uncertainties

All the rotation uncertainties are estimated using a segment-based bootstrapping method first described by Merkouriev & DeMets (2006) and modified herein as follows: From the 11 554 crossings of reversals C1n to C6n and the digitized traces of the four fracture zones and transform fault traces that are included in our data, we selected 1000 randomized data samples. Each randomized sample consists of four fracture zone flow lines and four transform faults selected randomly from the two strands of the Charlies Gibbs fracture zone, and the Bight and Molloy fracture zones and 21 sets of magnetic reversal crossings, each selected as follows. From the P palaeospreading segments that define the spreading centre for a given reversal, M segments were selected randomly such that $M = P$. All the reversal crossings for a given segment were added to the sample each time the segment was selected.

Via the randomized selection process, each palaeospreading segment, fracture zone and transform fault can be included multiple times within a given sample or may be excluded entirely. Since the weight that is given to the data that define a segment varies as the square root of the number of times the segment is included in the randomized sample, the 1000 randomized data samples capture a wider range of possible segment weightings than is the case for the original population of data. For long spreading centres that are populated by numerous data, as is true for the Eurasia-North America plate boundary, Merkouriev & DeMets (2006) find that rotation uncertainties that are determined via this method are significantly larger than the formal rotation uncertainties, which instead depend on the geometry of the reconstructed plate boundary and the assumption that data errors are random (Chang 1988; Royer & Chang 1991).

We inverted each of the 1000 sample data sets to estimate their best-fitting sequence of 21 finite rotations. The resulting 3-D scatter of the 1000 bootstrapped rotations for each of the 21 times represents a more conservative and (in our view) more realistic estimate of the finite rotation uncertainties. The covariances for each rotation are derived from the 3 × 3 orientation matrix for its 1000 bootstrap rotations (Fisher *et al.* 1993) and are given in Table 2. The best-fitting finite rotation for each of the 21 reversals is defined to be the average of its 1000 corresponding bootstrap rotations (Table 2). Following Gramkow (2001), we convert each bootstrap rotation to its equivalent quaternion and then find the renormalized mean of the 1000 rotations for each component of the quaternion. This method approximates the true mean within 1 per cent for rotations with angles smaller than 40 degrees (Gramkow 2001).

3.4 Calibration for outward displacement

Independent studies of near-bottom magnetic data (Sempere *et al.* 1987) and seafloor opening distances versus magnetic reversal ages (DeMets & Wilson 2008) indicate that the midpoints of magnetic polarity transition zones are shifted outward from their idealized locations by several kilometres nearly everywhere along the mid-ocean ridges. This outward displacement is caused by a variety

Table 2. Eurasia-North America plate motion rotations.

Chron	DOF	Lat. (°N)	Long. (°E)	Ω (degrees)	Covariances from bootstrap procedure					
					a	*b*	*c*	*d*	*e*	*f*
1n	996	−60.32	320.40	0.158	11.4	−1.8	7.5	3.9	0.0	44.0
2n	920	−63.65	315.80	0.363	43.7	22.5	11.9	38.7	−18.9	60.2
2An.1	1027	−63.81	318.16	0.538	38.4	7.0	20.2	27.9	−36.7	113.3
2An.3	878	−62.94	319.02	0.744	75.0	29.3	28.4	66.6	−44.7	110.0
3n.1	585	−62.38	317.91	0.858	159.9	22.5	79.5	38.7	−22.9	108.4
3n.4	650	−62.10	318.19	1.076	56.8	29.1	23.6	70.3	−33.8	91.3
3An.1	582	−62.68	315.93	1.222	69.2	15.3	28.7	51.6	−51.6	106.1
3An.2	522	−63.59	315.57	1.393	108.2	33.6	59.5	65.8	−29.0	128.7
4n.1	516	−63.56	317.83	1.574	119.9	41.8	48.9	66.3	−43.2	185.2
4n.2	569	−64.25	317.09	1.752	91.5	17.2	32.0	45.0	−59.3	165.2
4A	433	−64.64	315.91	2.017	132.3	16.3	71.8	56.4	−38.7	139.4
5n.1	564	−67.44	314.90	2.273	216.3	40.7	117.0	92.9	−70.7	396.3
5n.2	632	−68.18	313.90	2.613	109.5	29.2	53.2	94.4	−108.5	308.4
5An.2	386	−67.22	316.07	2.972	222.8	88.0	85.0	132.0	−60.9	286.8
5AC	246	−64.35	316.69	3.215	414.4	135.2	186.6	147.1	−72.3	419.5
5AD	218	−65.98	315.58	3.522	758.3	286.0	214.7	356.0	−240.4	854.2
5Cn.1	331	−68.06	315.87	4.011	776.8	519.5	−35.4	588.8	−185.4	338.7
5D	257	−68.20	314.84	4.327	1174.0	873.8	86.1	985.6	−144.3	419.3
5E	292	−69.05	313.69	4.623	938.8	501.5	106.0	464.5	−113.9	404.0
6ny	293	−70.71	311.30	4.927	206.7	−46.3	223.2	294.3	−441.9	1107.3
6no	386	−69.38	312.94	5.069	271.2	76.4	113.5	136.6	−115.6	500.2

The finite rotations reconstruct movement of the Eurasia plate relative to the North America plate and include location-dependent corrections for outward displacement described in the text. The rotation angles Ω are positive CCW. Each rotation is the mean of 1000 bootstrap solutions (see text). DOF, the degrees of freedom, equals the total number of anomaly, transform fault, and fracture zone flow-line crossings used to estimate the rotation for a given time reduced by the number of estimated parameters. The weighted rms misfits for these rotations are given in Table 1. The Cartesian rotation covariances are calculated in a Eurasia-fixed reference frame and have units of 10^{-10} radians^2. Covariances are determined from the bootstrapping procedure described in the text. Elements *a*, *d*, and *f* are the variances of the (0°N, 0°E), (0°N, 90°E), and 90°N components of the rotation. The covariance matrices are reconstructed as follows:

$$\begin{pmatrix} a & b & c \\ b & d & e \\ c & e & f \end{pmatrix}$$

of processes that collectively widen the zone within which new magnetic reversals are recorded in new oceanic crust along the mid-ocean ridges (Atwater & Mudie 1973). Barring any correction for outward displacement, rotations determined by reconstructing seafloor spreading magnetic lineations overestimate the underlying plate motion. For example, outward displacement of 5–6 km along the Reykjanes Ridge (Sempere *et al.* 1990; Merkouriev & DeMets 2008) comprises ≈30 per cent of the total distance between the old edges of C1n (0.78 Ma) flanking the ridge. Absent any correction for this outward displacement, an estimate of Reykjanes Ridge seafloor spreading rates from a reconstruction of C1n will give a spreading rate that is ≈30 per cent too fast.

Following procedures described by Merkouriev & DeMets (2006) and MD08, we estimate outward displacement at 16 distinct locations along the plate boundary. We first gathered all ≈4000 crossings of reversals 1n, 2n, 2An.1, 2An.3 and 3n.1 shown in Fig. 4 into 16 geographically distinct subsets. These five reversals span a long enough period of time (∼4 Ma) to define the recent opening rate for each area, but a short-enough period to increase the chances that no significant change in the opening rate will have occurred during this period (particularly in light of the evidence presented by MD08 for steady Eurasia-North America motion since 7 Ma). We inverted the reversal crossings from each area to find their best-fitting sequence of opening angles about the mean Eurasia-North America opening pole for these five reversals and converted the opening angles to equivalent best-fitting opening distances within each area. Finally, we inverted each of the 16 sequences of opening distances and their assigned reversal ages to find the best-fitting distance-axis intercept (Fig. 5) and opening rate for each area.

The distance-axis intercepts (Fig. 5) constitute our best estimates of the distance that two same-age magnetic lineations are displaced outward from the ridge relative to their idealized locations, provided that spreading rates have remained steady since C3n.1 (Merkouriev & DeMets 2008). All 16 distance-axis intercepts are greater than zero (Fig. 5), consistent with the systematic outward shift reported for many other spreading centres (DeMets & Wilson 2008). The intercept values range from 0.7 to 7.7 km, with the largest values (4.5 to 8 km) occurring along the Reykjanes Ridge. These results are consistent with values reported by MD08 and and agree well with polarity transition zone widths determined by Sempere *et al.* (1990) from inversions of deep-tow magnetic profiles across the Reykjanes Ridge at 63–63.6°N.

Given that many of the distance-axis intercepts are the same within their uncertainties, we evaluated the fits of two simpler descriptions of outward displacement. We tested but rejected a model in which the magnitude of outward displacement is required to remain constant along the plate boundary. Such a model more than triples the least-squares misfit to the 16 age-distance sequences and is rejected at high confidence level (≫99 per cent). Guided by the pattern shown in Fig. 5, we inverted the 10 age-distance sequences

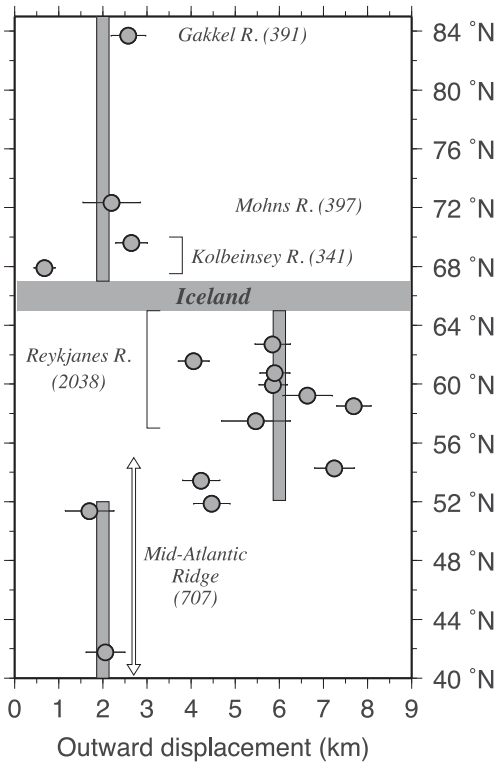

Figure 5. Outward displacement (circles) estimated from time sequences of seafloor opening distances reconstructed from crossings of C1no, C2n, C2An.1, C2An.3 and C3n.1 for 16 densely surveyed areas along the Eurasia-North America plate boundary. A distance-axis intercept (circle) and best-fitting opening rate (not shown) are determined from a weighted linear regression of each age-distance sequence. Numerals in parentheses specify the number of anomaly crossings that were reconstructed to find the opening distances within each area. The simplest pattern of outward displacement (vertical stippled bars) that fits the 16 opening-distance sequences within a predetermined statistical cutoff (1 per cent) consists of 6 ± 0.2 km of two-sided outward displacement between 52°N and Iceland and 2 ± 0.2 km everywhere else along the plate boundary.

from the magma-dominated ridge between 52°N and Iceland to estimate a single value for outward displacement in those areas and inverted the six age-distance sequences from elsewhere on the plate boundary to estimate a second value for outward displacement. The summed least-squares misfit for these two inversions does not differ significantly from that for the 16 separate inversions, indicating that the simpler two-valued model adequately fits the data. The inversions of the 10 age-distance sequences from magma-dominated segments of the ridge and the six age-distance sequences from elsewhere along the plate boundary give respective best estimates of 6 and 2 km for outward displacement, which agree well with our previous estimates of 5.5 and 2 km for the same parts of the plate boundary (Merkouriev & DeMets 2008).

All rotations in the ensuing analysis are corrected during the inversion process for outward displacement of 6 km at locations between 52°N and Iceland and 2 km elsewhere along the plate boundary. We refer to these corrected rotations as 'plate motion' rotations because they optimize estimates of the underlying plate motion. For comparison, rotations estimated by most authors optimize the superposition of magnetic lineations from both sides of the ridge without this correction and thus overestimate the underlying plate motion. For completeness, we estimate and tabulate both types of rotations (Tables 2 and 3). The misfits of both types of rotations to the data are compared Section 4.4.

4 RESULTS

We analysed the data in three stages. We first inverted the reversal, fracture zone and transform fault crossings everywhere along the plate boundary and examined the resulting reconstructions for obvious systematic misfits. We then determined the best-fitting sequence of plate motion rotations and uncertainties for the data that were retained from the first stage, evaluated the reconstruction misfits and used the best-fit pole locations, orthogonal rotation components and velocities for 1–3-Myr-long intervals between the present and 20 Mybp to describe in detail the Quaternary and Neogene histories of Eurasia-North America plate motion. Finally, we tested whether the numerous observations for the past ≈7 Ma are adequately described by a model that assumes Eurasia-North America motion has remained constant since ≈7 Ma.

4.1 Stage 1: data consistency

Systematic misfits to reconstructed magnetic lineations have several possible causes, including misinterpretations of the anomaly sequence for some spreading segments (a particular concern for the low-fidelity magnetic anomaly sequences that flank the Mohns and/or Gakkel ridges), local deviations in the magnitude of outward displacement from the values that are used to correct the rotations and discrete or distributed local or regional-scale deformation that affects part of a plate boundary. We thus begin the analysis by

Table 3. Eurasia-North America reconstruction rotations.

Chron	Lat.	Long.	Ω	Covariances from single inversion					
	(°N)	(°E)	(degrees)	*a*	*b*	*c*	*d*	*e*	*f*
1n	−64.22	319.69	0.216	21.0	−13.0	43.9	9.1	−28.2	103.7
2n	−59.48	309.23	0.388	24.3	−5.3	32.1	10.8	−19.5	66.6
2An.1	−62.35	310.43	0.569	18.2	−2.3	22.2	9.4	−14.6	50.1
2An.3	−60.40	314.13	0.760	19.2	−1.8	22.3	11.6	−15.1	49.9
3n.1	−60.93	313.30	0.882	34.8	−1.1	37.1	18.1	−23.9	80.7
3n.4	−60.38	316.03	1.097	30.4	−4.6	37.8	15.8	−23.3	79.0
3An.1	−61.90	312.98	1.253	32.2	−0.6	37.1	19.9	−23.8	81.8
3An.2	−62.38	312.32	1.414	38.8	−2.2	46.2	23.5	−29.6	101.8
4n.1	−63.03	314.22	1.599	39.5	−1.3	46.2	22.8	−31.8	112.2
4n.2	−63.58	313.82	1.775	38.0	3.6	40.0	23.0	−25.6	96.7
4A	−64.25	314.66	2.047	44.7	−6.0	64.6	24.1	−41.7	160.9
5n.1	−67.44	314.46	2.317	37.2	4.1	41.2	28.3	−35.5	144.6

Table 3 *(Continued)*

Chron	Lat.	Long.	Ω	Covariances from single inversion					
	(°N)	(°E)	(degrees)	*a*	*b*	*c*	*d*	*e*	*f*
5n.2	−68.30	312.57	2.662	33.3	−0.9	45.6	28.4	−39.2	150.8
5An.2	−66.70	315.32	2.997	146.8	−59.2	227.9	57.7	−140.9	484.7
5AC	−63.54	316.43	3.230	227.9	−110.2	404.9	100.5	−260.8	884.6
5AD	−65.40	315.16	3.537	228.7	−87.7	392.7	101.0	−243.4	872.6
5Cn.1	−67.27	315.41	4.017	124.4	−43.9	187.6	45.8	−105.3	381.2
5D	−67.47	315.40	4.335	167.5	−42.9	238.6	57.0	−115.4	468.0
5E	−68.38	314.13	4.641	180.5	−37.7	253.4	53.4	−115.5	491.2
6ny	−70.20	312.70	4.949	165.9	−22.3	218.2	47.4	−88.8	412.1
6no	−68.50	314.19	5.072	131.9	−45.1	208.1	44.1	−111.5	432.6

These finite rotations reconstruct reversals on the Eurasia plate onto their counterparts on the North America plate and exclude any corrections for outward displacement. The rotation angles Ω are positive CCW. Rotations and their covariances are determined from a single inversion of all the data. Table 2 specifies the degrees of freedom per rotation. Cartesian rotation covariances are calculated in a Eurasia-fixed reference frame and have units of 10^{-10} radians^2. See Table 2 caption for further information.

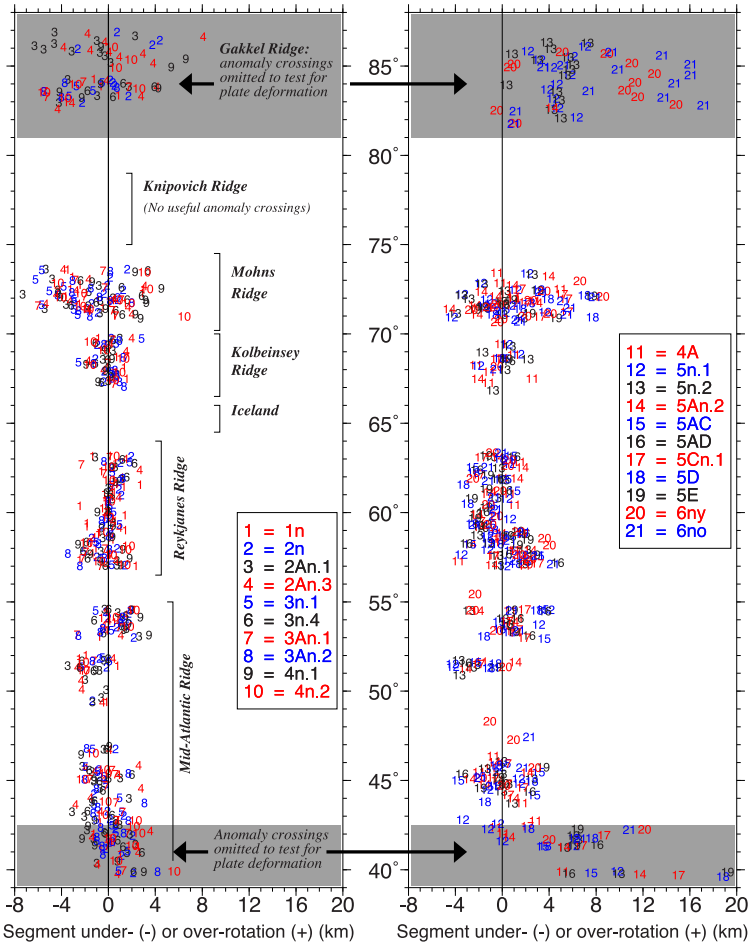

Figure 6. Search for systematic overrotations (positive) or underrotations (negative) of rotated reversal crossings relative to their stationary counterparts per reconstructed segment for C1no through C6no. Left-hand panel shows the segment misfits versus segment latitude for 947 spreading segments for C1no through 4n.2. Right-hand panel shows misfits for C4A through C6no. The misfit for each segment is the weighted average misfit for the ensemble of reconstructed reversal crossings that define the segment.

inverting the observations for all 21 reversals and examining the resulting reconstructions for obvious misfits or outliers. We found only two subsets of the data with systematic misfits, one consisting of reversal crossings older than C3An.1 within ≈200 km of the Azores triple junction and the other consisting of all reversal crossings older than C4n.2 from the Gakkel Ridge. To better understand these misfits, we re-inverted the observations while excluding both of these data subsets and used the resulting best-fitting rotations to reconstruct all the data, including the two omitted data subsets.

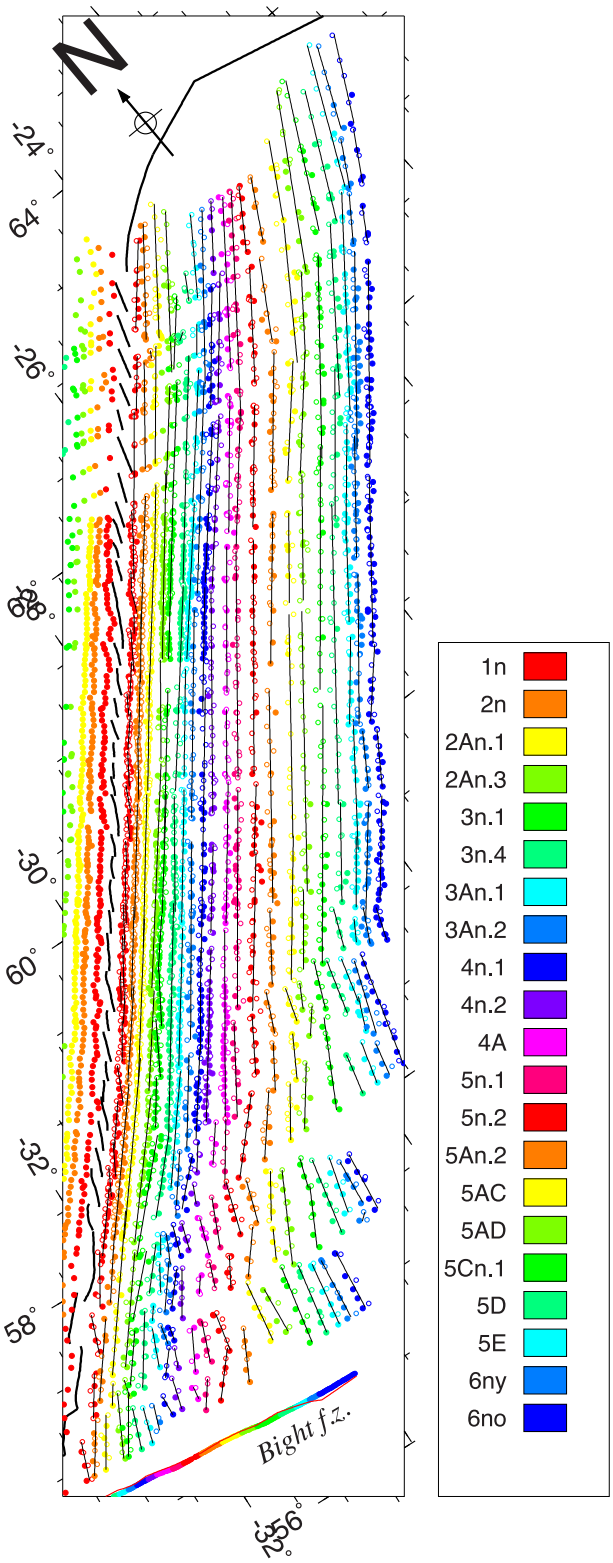

Figure 7. Reconstructions of the Reykjanes Ridge magnetic anomaly crossings. Filled circles show anomaly crossings at their original, unrotated locations on both sides of the ridge. Open circles show magnetic reversal crossings from the North America plate reconstructed to their positions on the Eurasia plate with the best-fitting rotations in Table 2. Bold line shows the ridge axis. Thin black lines show the great circle segments that best fit the reconstructed reversal crossings. Projection is oblique Mercator about a pole ninety degrees from the Reykjanes Ridge along the great circle locally parallel to the Reykjanes Ridge magnetic lineations.

Fig. 6 summarizes the segment misfits as a function of latitude along the plate boundary, where a single segment misfit is defined as the average overrotation (positive values) or underrotation (negative values) of the rotated reversal crossings with respect to the stationary crossings that define the segment.

For crossings of C1n through C3An.1 (left-hand panel of Fig. 6), we find no evidence for regionally coherent, systematic misfits anywhere along the plate boundary. The typical segment misfits for C1n to C3An.1 are smaller than several km (Fig. 6) except along the Gakkel and Mohns ridges, where we attribute the modestly larger scatter to their lower-fidelity magnetic anomaly sequences. Based on these good fits, we conclude that our correlations of C1n through C3An.1 are correct everywhere along the plate boundary, that our corrections for outward displacement are approximately correct, and that neither the Eurasia nor North America plates has deformed significantly in the Arctic region or northern Atlantic since C3An.1. Consequently, all of the C1n to C3An.1 reversal crossings are used below to estimate Eurasia-North America rotations.

For reversals older than C3An.1 (denoted by numerals 8–21 in Fig. 6), reconstructions of the lineations between the Azores triple junction and 42°N gives rise to persistent overrotations that increase in magnitude from ∼4 km for C3An.2 (6.7 Ma) to nearly 20 km for C5E (18.1 Ma). The time-dependent misfits are roughly equivalent to a 1 mm yr^{-1} spreading-rate deficit across the Mid-Atlantic Ridge south of 42°N between 19.7 and 6.7 Ma relative to the predicted Eurasia-North America spreading rate. Diffuse deformation associated with Azores triple junction may have extended farther north before 6.7 Ma than is presently the case (Marques *et al.* 2013). In light of these misfits, all identifications of C3An.2 through C6no from locations south of 42°N are omitted from our determinations of Eurasia-North America rotations.

Along the Gakkel Ridge, C5n.1 and C5n.2 are overrotated by 4–6 km and C6ny and C6no by 8–16 km (denoted by numerals 12 to 21 in Fig. 6). Given the low fidelity of the Gakkel ridge anomaly sequence, misidentifications of these magnetic anomalies could be the source of these misfits or the misfits may have a tectonic origin, as suggested by the increase in misfit with reversal age. The misfits for C6ny and C6no are a factor-of-two or more larger than misfits elsewhere along the plate boundary (Fig. 6). We thus exclude all Gakkel Ridge crossings of C6no and C6ny from our determinations of the Eurasia-North America rotations. We retained the Gakkel Ridge crossings of C5n.1 and C5n.2 for our Eurasia-North America rotation estimates because the misfits to both reversals are no larger than those along the Mohns Ridge and other locations farther south.

4.2 Stage 2: best-fitting rotations, reconstructions and kinematic history

The best-fitting Eurasia-North America rotations (Table 2) are determined from a simultaneous inversion of 13 244 magnetic reversal, fracture zone and transform fault crossings (Fig. 4) and are corrected for 6 km of outward displacement between Iceland and 52°N and 2 km elsewhere along the plate boundary (Section 3.4). For the convenience of some readers, we inverted the same data while omitting any correction for outward displacement (Table 3). These rotations optimize the magnetic lineation reconstructions in the traditional sense used by many authors, but are biased with respect to the plate motions (particularly for young anomalies). All rotation covariances are determined via segment-based bootstrapping, as described in Section 3.3.

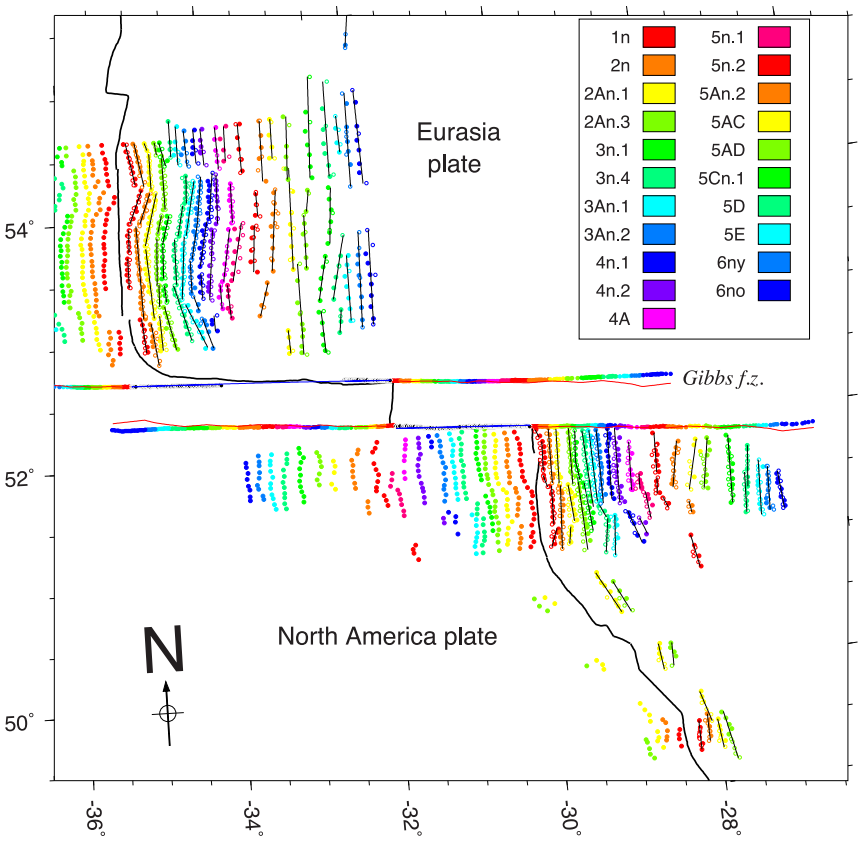

Figure 8. Reconstructed magnetic lineations, transform fault small circles and fracture zone flow lines for the Mid-Atlantic Ridge, 48°N to 55°N. Blue lines show small circles about the best estimate for the C1n rotation pole, which is optimized to fit the transform fault trace. Red lines show the fracture zone flow lines predicted from stage rotations determined from the best-fitting finite rotations in Table 2. See caption to Fig. 7 for further information and Fig. 4 for figure location.

4.2.1 Reconstructed magnetic lineations and flow lines

Figs 7 to 12 show reconstructed magnetic lineations for the whole plate boundary. The high-fidelity Reykjanes Ridge magnetic lineations (Fig. 7) and clear magnetic anomaly sequence near the Charlie Gibbs fracture zone (Fig. 8) strongly constrain the rotation estimates and are well fit by the rotations. Improvements in the magnetic anomaly coverage between the Azores triple junction and 46°N (Fig. 9) relative to our previous study (MD08) help to better define the best-fitting pole locations and reduce uncertainties relative to those from MD08. The magnetic lineations along the Kolbeinsey Rise (Fig. 10) are also well fit except for C6ny, for which the only crossing we identified west of the ridge axis is poorly aligned when rotated onto the Eurasia plate.

Along the Mohns Ridge, the reconstructed magnetic lineations (Fig. 11) comprise a relatively complete sequence except for C5AC and C5AD, which we were unable to identify with enough confidence to include in the analysis. Significant scatter in the orientations of some reconstructed lineations along the Mohns Ridge is a likely effect of the lower-fidelity and hence less well-determined reversal locations. The reversal sequence reconstructed along the Gakkel Ridge (Fig. 12) is even less complete than for the Mohns ridge; all reversals older than C5n.2 are omitted (see above) and the scatter in the Gakkel Ridge segment misfits is larger than elsewhere along the plate boundary (Fig. 6). Despite these problems, the Mohns and Gakkel Ridge data add useful new information to our rotation estimates because they define the total seafloor opening at locations nearer the pole than any of the other data and thus improve our estimates of the along-ridge opening gradient for many of the 21 reversals.

Fig. 13 shows flow lines on the Eurasia and North America plates that are reconstructed from stage rotations determined from the best-fitting finite rotations (Table 2). The reconstructed fracture zone flow lines (red lines in Fig. 13) and transform fault small circles (blue lines in Fig. 13) are generally located within a few kilometres of their observed traces. Given the difficulty in defining where palaeoslip occurred within a fracture zone valley, we consider the flow-line fits to be acceptable. The 1377 fracture zone crossings have $\hat{\kappa} = 1.59$, indicating that the uncertainties we estimated in the locations of the fracture zone crossings are ~25 per cent too large. For the 313 transform fault crossings, $\hat{\kappa} = 9.6$, indicating that the average misfit of ≈500-m is three times smaller than the average assigned uncertainty. The good fits to the crossings of the Gibbs, Bight and Molloy transform faults and fracture zones not only indicate that they impose a consistent set of constraints on the best-fitting rotations, but that both types of data are also consistent with the constraints that are imposed by the more numerous magnetic reversal crossings (which comprise nearly 90 per cent of the data).

Variations in the trends of the predicted flow lines clearly occur along strike (Fig. 13), often in disagreement with their more smoothly varying digitized flow lines. These along-strike variations are a by-product of small adjustments to the best-fitting finite rotations that occur during the inversion procedure in order to optimize

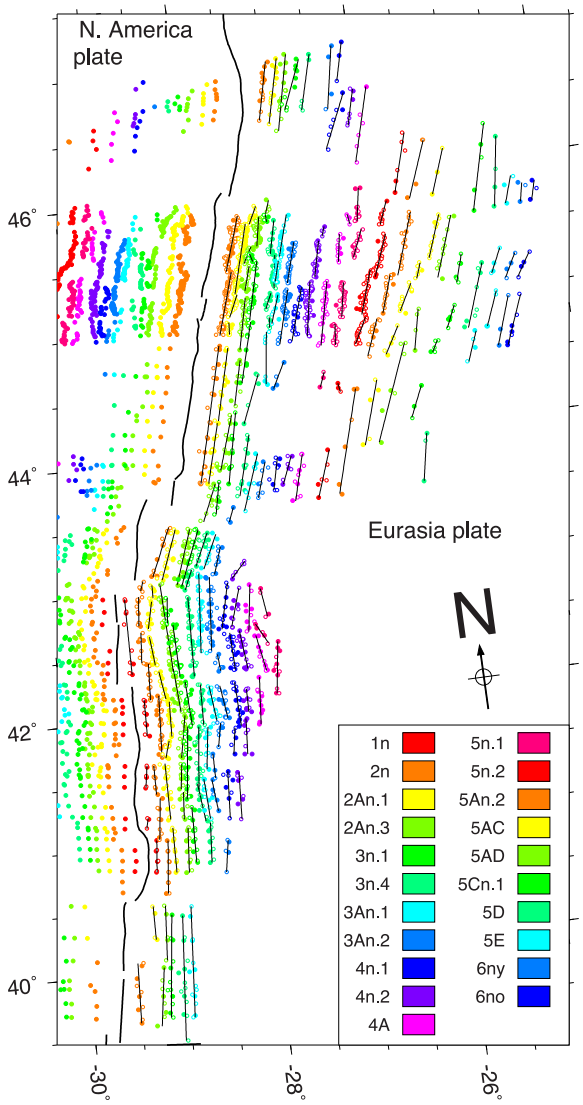

Figure 9. Reconstructed magnetic lineations from the Azores triple junction to 47°N. Projection is oblique Mercator around a pole at 66°N, 137°E, the mean location of the best-fitting Eurasia-North America poles for C1n through C3An.1. See caption to Fig. 7 for further information and Fig. 4 for figure location.

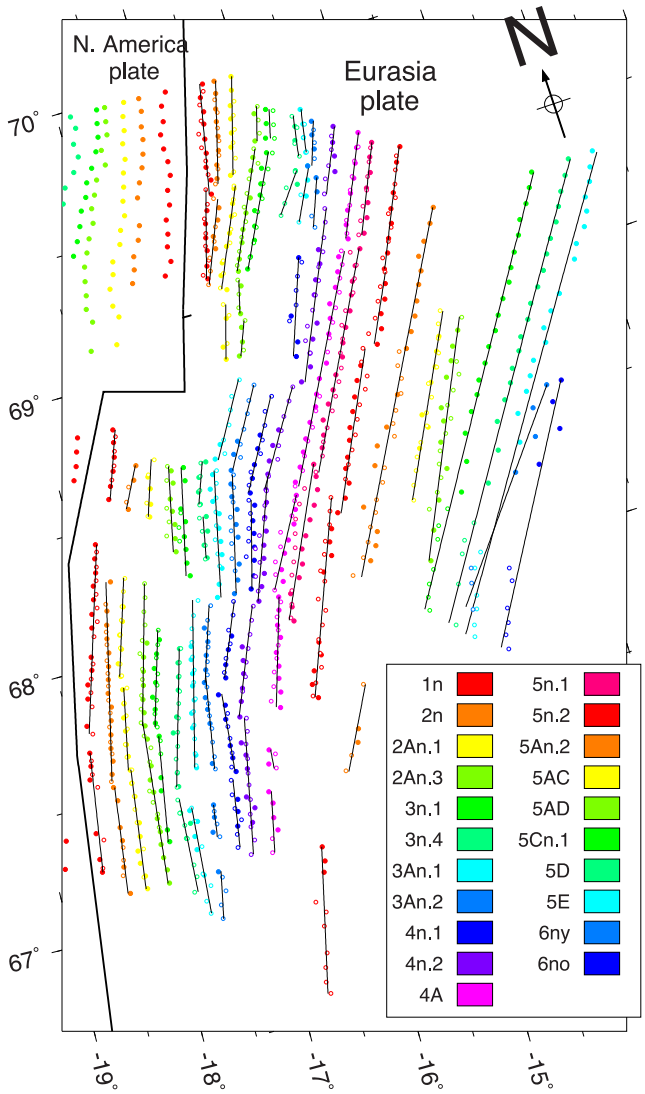

Figure 10. Reconstructed magnetic lineations along the Kolbeinsey Ridge north of Iceland. See caption to Fig. 7 for further information and Fig. 4 for figure location.

the fit to the numerous magnetic reversal crossings. As an experiment, we increased the weighting of the fracture zone crossings to find rotations that yielded more smoothly varying flow lines. Although this succeeded, unrealistically small uncertainties in the fracture zone locations (several hundred metres) were needed to generate smooth flow lines and the reconstructed reversal crossings were fit significantly worse than by the best-fitting rotations in Table 2. We thus retained our originally assigned fracture zone uncertainties.

At the start of our analysis, we included the Jan Mayen transform fault and fracture zone to help determine best-fitting Eurasia-North America rotations. We found however that neither is inconsistent with the plate slip history determined from Charlie Gibbs, Bight and Molloy fracture zones. For example, on the Eurasia plate east of the ridge axis, a flow line determined for the Jan Mayen fracture zone from the best-fitting rotations in Table 2 (Fig. 13) is located several kilometres systematically north of the flow line that we digitized within the altimetrically defined fracture zone valley. On the North America plate (west of the ridge), the predicted flow line is located south of our digitized flow line (Fig. 13) and instead follows a linear bathymetric feature that may mark the correct fracture zone location. We suspect that our interpretations of the fracture zone locations on one or both sides of the ridge do not accurately track the locus of palaeoslip and thus elected not to use the Jan Mayen transform fault or fracture zone to estimate the best-fitting rotations.

4.2.2 Misfits to individual data types and spreading segments

Overall, $\hat{\kappa} = 0.998$ for the 13 244 magnetic reversal, fracture zone, and transform fault crossings that were inverted to determine the 21 best-fitting rotations. This differs insignificantly from the value of 1.0 that is expected for observations whose uncertainties are approximately correct. The rms misfits to the individual reversal crossings increase gradually from 1.2 km for C1no and other young reversals (Fig. 14) to 2.0 km for the oldest reversals.

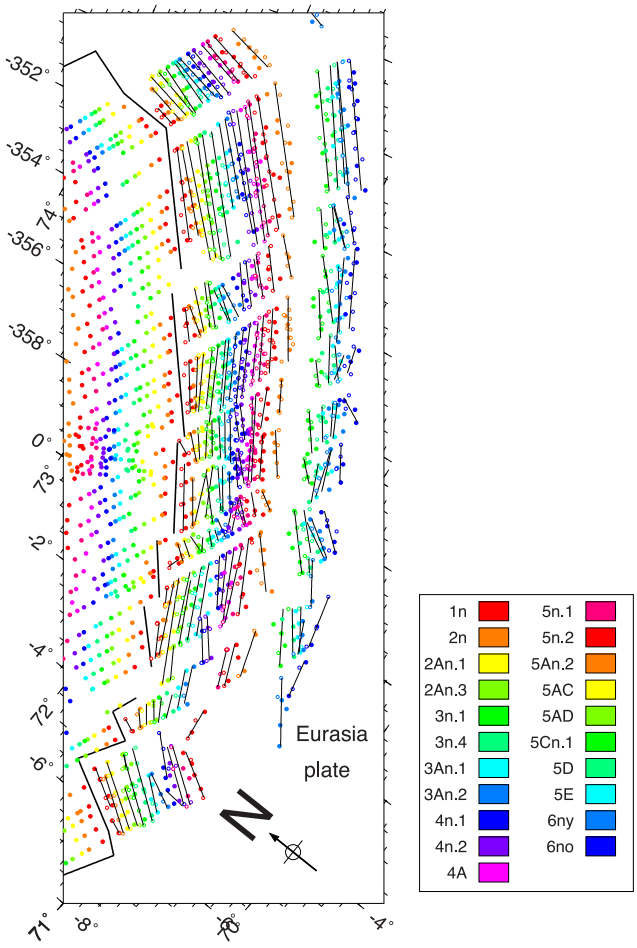

Figure 11. Reconstructions of magnetic lineations along the Mohns Ridge in the Arctic Basin. Projection is oblique Mercator about a pole 90° from the Mohns ridge along the great circle locally parallel to the Mohns Ridge magnetic lineations. See caption to Fig. 7 for further information and Fig. 4 for figure location.

The distribution of the weighted misfits is Gaussian (Fig. 15a) and has a dispersion of 1.7 km (red lines in Fig. 15b). The misfits along the ultraslow-spreading Mohns and Gakkel ridges are modestly larger than elsewhere along the plate boundary (Fig. 15b), most likely due to the lower resolution of the magnetic anomaly sequences along those ridges.

The rms misfits to the fracture zone crossings range from 0.3 to 2 km for reversals younger than C5AD (Fig. 14), but increase rapidly to 7 km for crossings associated with the oldest reconstructions. We attribute the larger misfits for the oldest reconstructions to the difficulty of identifying the precise location of palaeoslip at progressively older reconstruction ages.

Fig. 15(c) summarizes the overrotation or underrotation of each reconstructed palaeospreading segment relative to its stationary-side segment. For the 947 reconstructed spreading segments, the rms segment-specific misfit averages 2 km (red lines in Fig. 15c). For comparison, simulations of the expected rms segment-specific misfit given reversal crossings with random (Gaussian) location errors of 1.7 km indicate that the rms over or underrotations per segment should be only 0.7 km (Merkouriev & DeMets 2006). The larger-than-expected segment misfit thus indicates that errors in locating the position of a magnetic reversal include both a random component (Fig. 15A) and a component correlated between the

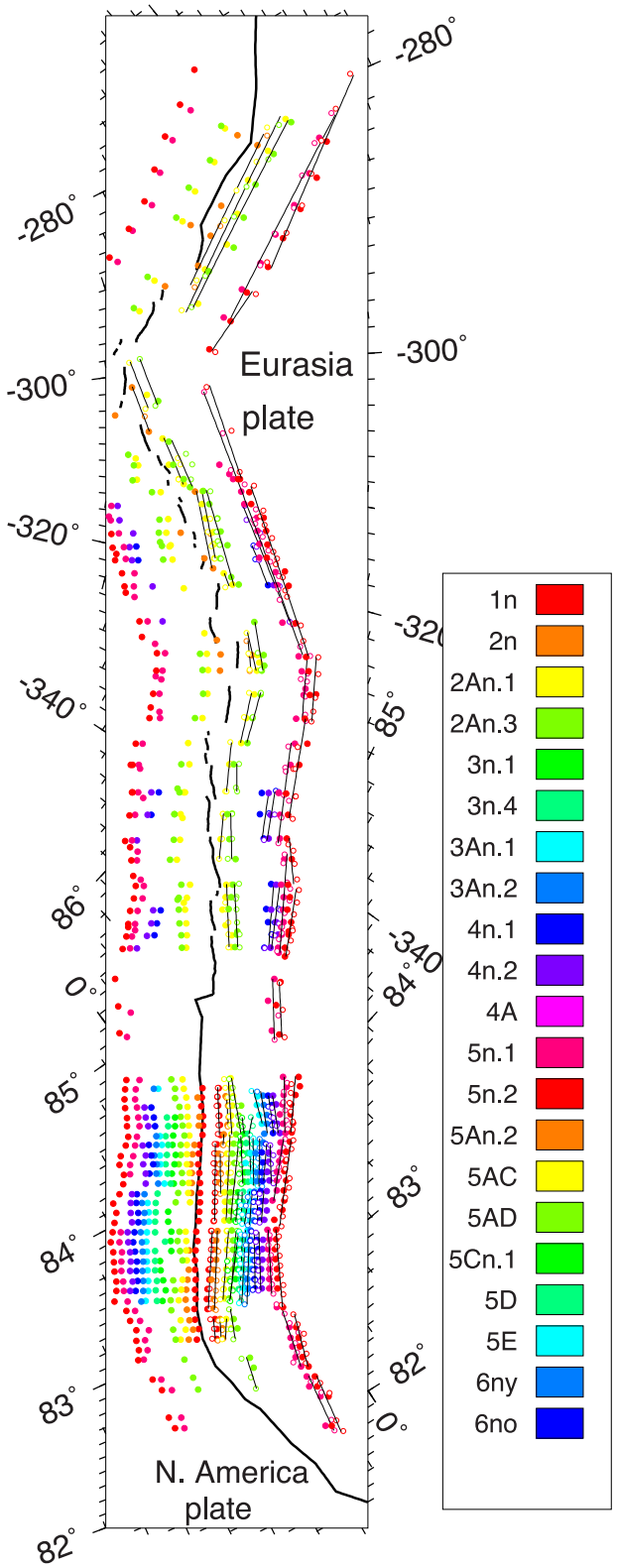

Figure 12. Reconstructions of magnetic lineations along the Gakkel Ridge in the Arctic Basin. See caption to Fig. 7 for further information and Fig. 4 for figure location.

crossings from a given spreading segment. This corroborates similar findings from reconstructions of magnetic anomalies from the India-Somalia and Nubia-North America plate boundaries (Merkouriev & DeMets 2006, 2014).

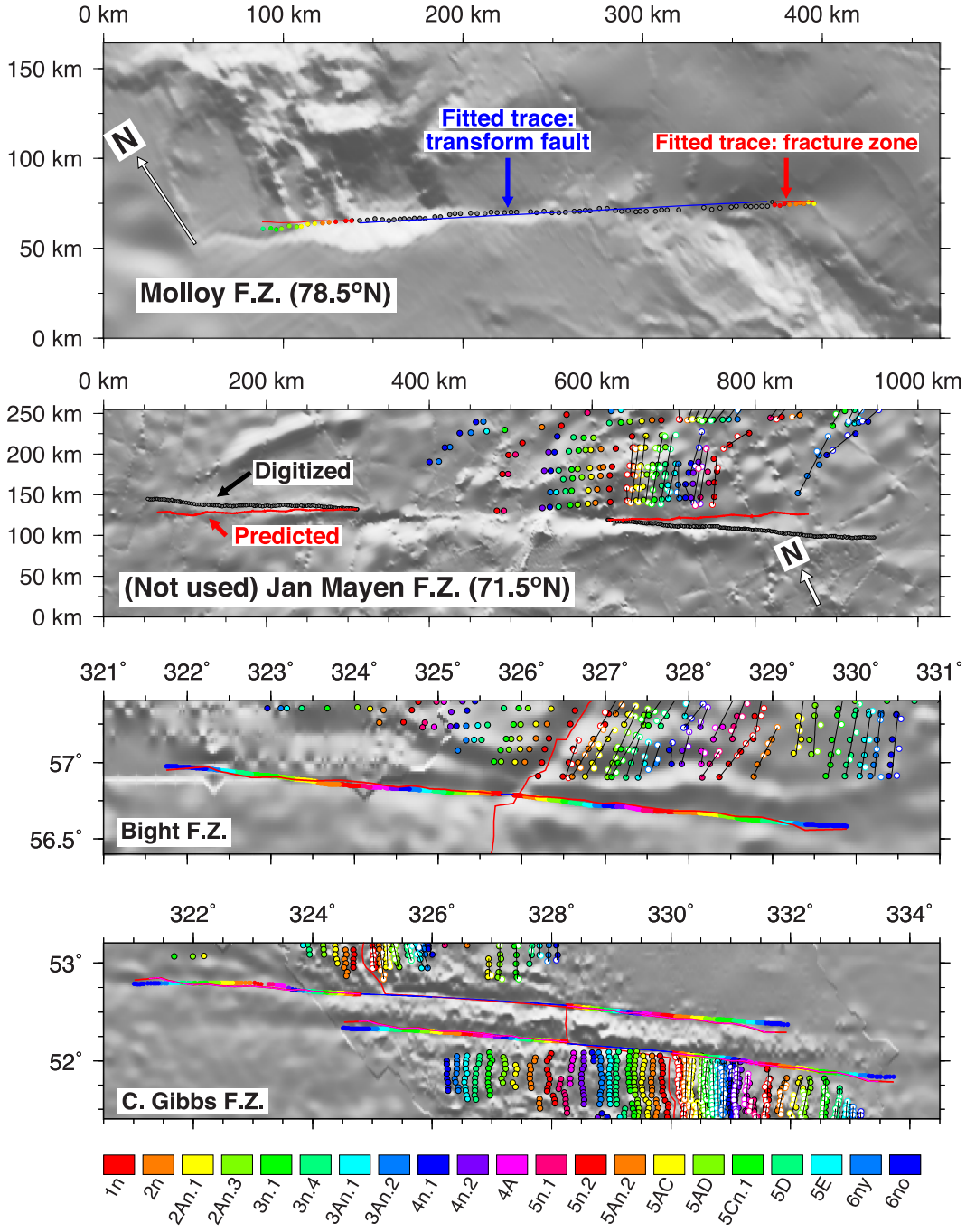

Figure 13. Flow lines predicted for Eurasia-North America fracture zones (red) and transform faults (blue). The digitized traces of the Molloy, Bight and Charlie Gibbs fracture zones (circles) were used to estimate the best-fitting Eurasia-North America rotations. Red lines show the fracture zone flow lines reconstructed from stage rotations determined from the best-fitting rotations. The best-fitting traces for the transform faults are small circle segments (blue lines) about the pole for C1n. The trace predicted for the Jan Mayen fracture zone, which was excluded from the inversion, is also shown. Colour scale for the reversal and fracture zone crossings appears below the maps. Upper two maps are oblique Mercator projections about the average Eurasia-North America pole since 5 Ma.

4.2.3 Influence on the fit of the correction for outward displacement

The best-fitting rotations in Table 2, which incorporate the 2 and 6-km corrections for outward displacement described in Section 3.4, have a cumulative least-squares misfit χ^2 of 11 306. For comparison, the best-fitting rotations in Table 3, which are not corrected for outward displacement, have $\chi^2 = 12\,930$. The ≈15 per cent improvement in fit associated with the two corrections for outward displacement is significant at confidence levels much greater than 99 per cent as determined using an F-ratio test for two additional model parameters. We conclude that the corrections for outward displacement are strongly justified by the improvement in fit to the numerous observations.

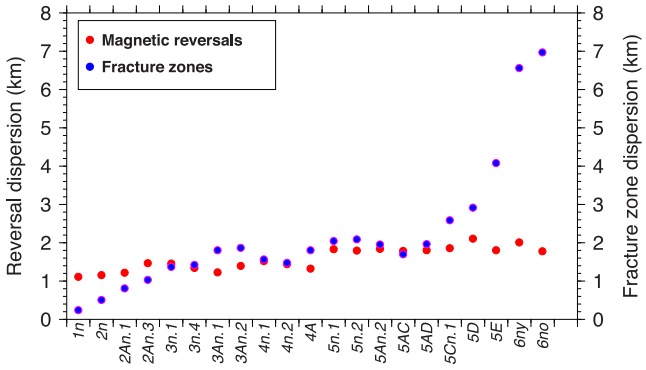

Figure 14. Weighted rms misfits in kilometres of the best-fitting rotations to magnetic reversal and fracture zone crossings per magnetic reversal. Each fracture zone crossing is retroactively assigned an approximate age by matching it with its nearest-neighbour point along its corresponding predicted plate flow line.

4.2.4 Pole locations

The 21 best-fitting Eurasia-North America poles are clustered between 60°N and 71°N (Fig. 16). For reversals younger than C4A, the poles cluster strongly around 63°N, 137°E (Fig. 16), ≈500 km south of the poles for reversals older than C4n.2, which are clustered near 68°N, 135°E (Fig. 16). These suggest that the pole moved to its present position at ≈8–7 Ma. We later test whether the pole has remained stationary for the past 7 Myr.

Our pole locations for C5 and C6 are similar to those reported by many previous authors (e.g. Pitman & Talwani 1972; Talwani & Eldholm 1977; Srivastava & Tapscott 1986; Rowley & Lottes 1988; Lawver *et al.* 1990; Gaina *et al.* 2002; Glebovsky *et al.* 2006). More detailed comparisons between our own and previous results are given in the following Section 5.

4.2.5 Motion change after ∼8 Ma

A reconstruction of opening distances for all 21 times along the Reykjanes Ridge (at 59.2°N, 29.4°W) clearly shows evidence for one significant slowdown in the rate of seafloor accretion (Fig. 17a) at ∼8–6.5 Ma, consistent with the slowdown in at 7±1 Ma first described by MD08. This is discussed further below.

The time sequence of angular distances between the Eurasia-North America stage poles and the Reykjanes Ridge reference point (Fig. 17b) indicates that at ∼9–8 Ma, the stage opening pole migrated southward away from plate boundary by 10–12 angular degrees (1100–1300 km), consistent with the timing implied by the finite opening pole sequence shown in Fig. 16. From 8 Ma to the present, the same observations suggest (but do not require) that the opening pole has continued to migrate southward (Fig. 17b), although not by more than 3-4 angular degrees.

4.2.6 Eurasia-North America interval velocities

Fig. 18 documents the Quaternary and Neogene evolution of seafloor spreading rates and plate slip directions for a flow line along the Reykjanes Ridge, where the high-fidelity magnetic anomaly sequence gives the best-determined interval velocities along the plate boundary. The interval spreading rate history is predicted by stage rotations derived from the plate motion rotations in Table 2. The intervals we selected typically last one to three million years,

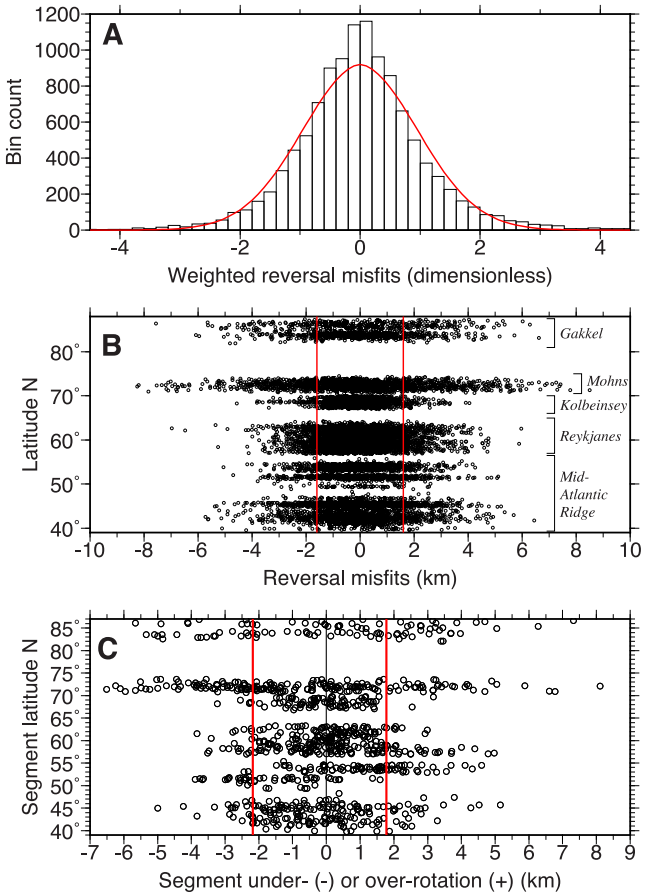

Figure 15. Data misfits. (a) Histogram of misfits for all 11 554 reconstructed Eurasia-North America reversal crossings normalized by their estimated uncertainties. Red curve shows the Gaussian distribution of weighted residuals expected for an equivalent number of degrees of freedom (11 554 minus 1936, the number of parameters used to fit the observations) for data with normally distributed errors and correctly estimated uncertainties. (b) Reversal crossing misfits in kilometres versus plate boundary latitude. The vertical red lines in (b) encompass 68.3 per cent of the misfits after adjusting for the number of estimated parameters. They thus indicate the overall dispersion of the reversal crossings relative to their best-fitting great circle segments. (c) Over and underrotations of the 947 rotated anomaly segments with respect to their fixed-side segment counterparts for Chrons 1-6no. The vertical red lines show the expected magnitude of the systematic misfits for simulated reversal crossings with random, but no systematic noise in their locations.

long enough to reduce uncertainties in the stage velocities to under ±1 mm yr^{-1} (Section 3.1).

The stage spreading history (Fig. 18) clearly shows the change in plate motion at 6–7 Ma first described by MD08 and indicated in Fig. 17. From the present back to 6.7 Ma, the interval rates typically vary by less than ±3 per cent from their 6.7-Ma-average rate of 19.2 ± 0.5 mm yr^{-1}, strongly suggesting that spreading rates have remained steady since 6.7 Ma. Interval seafloor spreading rates from 19.7 to 6.7 Ma also typically vary by less than 1 mm yr^{-1} from their pre-6.7-Ma-average of 23.7 ± 1 mm yr^{-1}.

The interval slip directions show no clear evidence for a significant change since 20 Ma (Fig. 18b). Most of the scatter in the estimated slip directions is noise that results from small differences in the finite pole locations that are driven by fitting of the magnetic reversal crossings, which far outnumber the fracture zone crossings and thus carry more weight in the inversion.

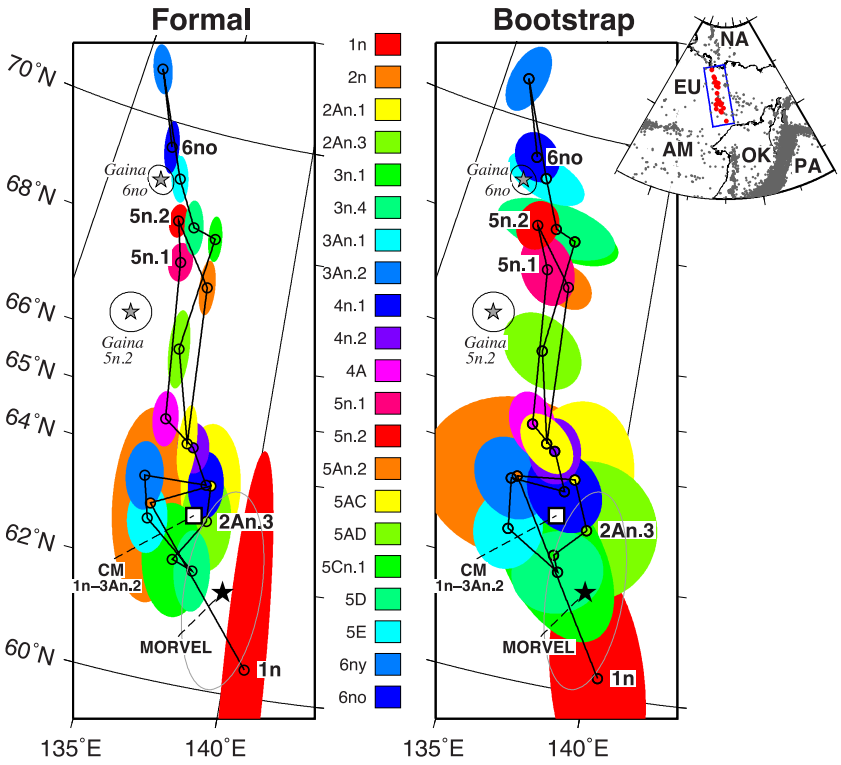

Figure 16. Eurasia-North America plate motion poles and 2-D 95 per cent confidence regions for magnetic reversals 1n to 6no. In the inset map, the blue rectangle shows the location of the larger panels, the red circles show locations of Eurasia-North America plate motion poles, and the grey circles show shallow earthquake locations, 1963 to 2010. The left-hand panel shows the best-fitting poles from a single inversion of the data and the formal uncertainty regions propagated from the geometric and data uncertainties (Chang 1988). The right-hand panel shows our preferred model (Table 2), whereby the best-fitting poles and confidence regions are determined from inversions of numerous randomized data samples (see text). The open square labelled 'CM 1n-3An.2' is the best constant-motion pole for the past 6.7 Myr, as described in the text. Star shows the 3-Myr-average MORVEL Eurasia-North America pole and 95 per cent confidence ellipse (grey line). Grey stars are poles from Gaina *et al.* (2002). Plate abbreviations are AM, Amuria Plate; EU, Eurasia; OK, Okhotsk; NA, North America; PA, Pacific.

In summary, the plate motion rotations are consistent with steady motion from 20 to 7 ± 1 Ma, a ∼20 per cent slowdown in Eurasia-North America motion at 7–6 Ma, and steady motion from ≈6 Ma to the present. Near the Azores triple junction, seafloor spreading rates slowed by ∼25 per cent (Fig. 19) at 7 Ma. The spreading slowdown was smaller along the Kolbeinsey Ridge north of Iceland (Fig. 19) and almost no detectable change occurred along the Gakkel Ridge (Fig. 19). Given the difficulty in identifying magnetic reversals from the low-fidelity magnetic data from the Gakkel Ridge, we are less confident in the details of its spreading history than for other locations along the plate boundary.

4.3 Stage 3: testing simpler models for Eurasia-North America motion

We conclude the analysis by testing the hypothesis that Eurasia-North America motion has remained constant since C3An.2 (6.7 Ma). We first examine whether the data for C1no through C3An.2 are well fit if we require the rotation pole to remain stationary from the present back to C3An.2, but permit the rate of angular rotation to change through time. We then test whether the same data are well fit if we enforce both a stationary rotation pole and constant angular rotation rate. Hereafter, we refer to the latter as the constant-motion model.

4.3.1 Test for a stationary pole

We first test the fit of a model that describes Eurasia-North America motion since 6.7 Ma with a single rotation pole and eight independent opening angles, one for each of the eight reversals between and including C1no and C3An.2. An inversion of the 7245 data for these eight reversals gives a best-fitting pole of 63.0°N, 137.8°E, near the centre of the individual poles for these reversals (Fig. 16). The weighted root mean square (wrms) data misfits for the eight reversals increase by no more than 1 per cent or 10–15 m (0.01–0.015 km) relative to the misfits for the best-fitting rotations (Table 2). Consequently, there is almost no fitting penalty incurred by requiring the rotation pole to remain stationary since 6.7 Ma. The interval plate velocities predicted by this model (black circles in Fig. 18) do not differ significantly from those estimated from the best-fitting rotations.

4.3.2 Test for constant plate motion

An inversion of the same 7245 data to determine a best stationary pole and constant angular rotation rate for the past 6.7 Myr gives 63.1°N, 137.7°E, 0.206° Myr^{-1} for the Eurasia plate relative to North America. The pole differs insignificantly from the best stationary pole described above. The wrms misfits are only 0–40 m larger (3 per cent or less) than for the eight best-fitting rotations in Table 2, an insignificant fitting penalty. For a location on the

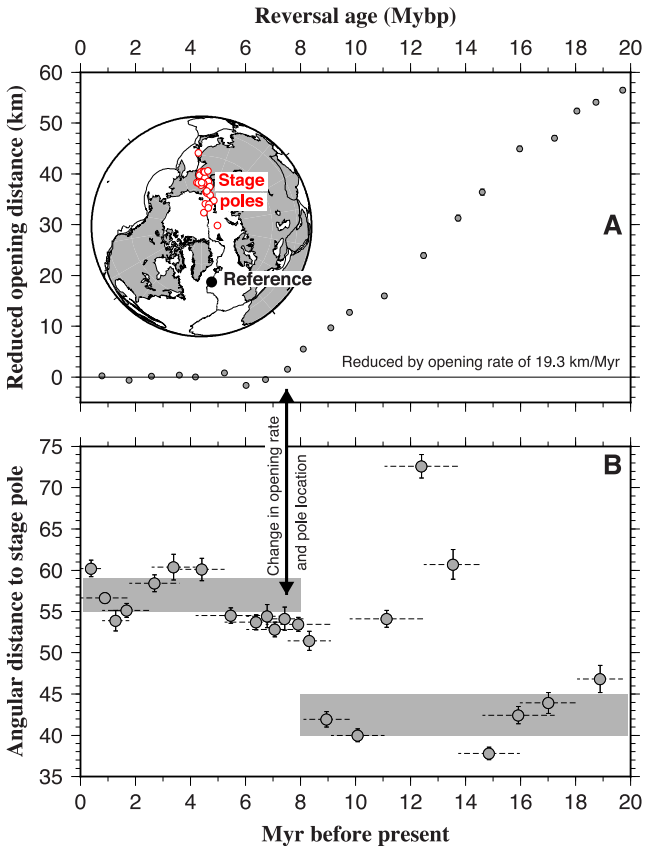

Figure 17. Evidence for changes in Eurasia-North America seafloor spreading rates (a) and stage pole locations (b). Panel A shows reduced seafloor distances versus time for a reference point along the Reykjanes Ridge. The reduced distance is the total opening distance predicted from the rotations in Table 2 reduced by the best average opening rate (19.3 km per Myr) that is predicted by the constant-motion rotation for the present back to 6.7 Ma (Section 4.3.2). Panel B shows the angular distance from each Eurasia-North America stage pole to the Reykjanes Ridge reference point shown on the inset globe. The time intervals that are spanned by the stage poles are indicated by the horizontal dashed lines in (b). The stage poles for times after 9–7 Ma migrated 10–15 degrees farther from the plate boundary than the older stage poles, roughly consistent with the timing in the change in the opening rate.

Reykjanes Ridge, the spreading rate and plate direction estimated with the constant-motion model (Fig. 18) differ by no more than ± 0.5 mm yr^{-1} (± 2 per cent) and 2.5° from the interval velocities estimated from the best-fitting rotations (Table 2).

The evidence thus suggests that Eurasia-North America motion has been steady for the past 6.7 Ma about a pole centred at 63.1°N, 137.7°E, with an angular rotation rate of 0.206° Myr^{-1}.

5 DISCUSSION

5.1 Comparison to results of Merkouriev & DeMets (2008)

In our previous study (Merkouriev & DeMets 2008), we found that Eurasia-North America seafloor spreading rates slowed by 20 ± 2 per cent at 7.5–6.7 Ma and the pole migrated 650 km southwards from a pre-7.5 Ma position near 70°N, 127°E to a location near 64°N, 137°E. Here, we confirm both the timing and magnitude of the decline in seafloor spreading rates at 7–6 Ma along much of the Eurasia-North America plate boundary, but find that the southward shift in the pole location at 7–6 Ma was even larger than we previously estimated. Our new results indicate that the Eurasia-North America stage pole was located near 71–72°N, 130–132°E before 6.7 Ma, ≈1000 km north of the pole location since 6.7 Ma. As discussed by Merkouriev & DeMets (2008), the southward pole migration at 7–6 Ma changed the convergent stress regime that prevailed across large areas of northeastern Asia before 6.7 Ma to an extensional regime across areas located south of 71–72°N. The forces that caused the large and apparently rapid southward movement of the pole remain unknown.

Our new results complement those of our previous study in four ways. First, they demonstrate that magnetic data from the Arctic Basin spreading centres are mostly consistent with the Eurasia-North America plate kinematic history determined in our previous study, which relied largely on data from outside the Arctic Basin. Second, our new results suggest that Eurasia-North America slip directions have not changed significantly since 20 Ma, contrary to our previous conclusion that opening direction rotated several degrees anti-clockwise at 7 Ma. Third, our updated estimate of the location of the pole for the past 0.78 Myr is now consistent with the poles we estimate for other reversals younger than 7 Ma (Fig. 16). In contrast, our previous estimate of the C1no Plate motion pole was located nearly 700 km north of the poles we estimated for other young reversals.

Finally, we find for the first time evidence for systematic misfits for C5n.1 and older anomalies along the Gakkel Ridge (Fig. 6), possibly indicating that slow microplate deformation or distributed deformation within the Eurasia or North America plates occurred at high latitudes before 10 Ma. The systematic misfits range from several km to ∼20 km and increase with anomaly age during the ≈10-Myr-long interval between C5n.1 and C6no. This implies that any such deformation was slow, equivalent to a 1 mm yr^{-1} spreading deficit across the Gakkel Ridge relative to that expected for Eurasia-North America motion. Similar small misfits to anomalies 4A and older north of the Azores triple junction may also be evidence for slow deformation related to the Azores microplate.

5.2 Comparison to results from Gaina *et al.* (2002)

Gaina *et al.* (2002) use reversal crossings extracted from the Arctic and north Atlantic magnetic anomaly grid (Macnab *et al.* 1995; Verhoef *et al.* 1996) and fracture zone crossings from the marine gravity grid of Sandwell & Smith (1997) to estimate Eurasia-North America rotations for C5n.2, C6no and many older reversals. Their poles for C5n.2 and C6no agree well with our own estimates (right-hand panel of Fig. 16) and confirm that Eurasia-North America poles before C4n.2 were located significantly farther north than their present location near 63 °N. The total opening distances that are predicted across the Reykjanes Ridge by our best-fitting rotation for C5n.2 (Table 3) and that of Gaina *et al.* (2002) differ by only 2.4 km (1 per cent). Similarly, the two models predict total opening distances for C6no that differ by only 1.6 km (0.4 per cent). The good agreement between these independent estimates suggests that Eurasia-North America reconstructions for C5n.2 and C6no are accurate to within a few kilometres at 95 per cent uncertainty.

5.3 Comparison to MORVEL results

The MORVEL Eurasia-North America angular velocity describes seafloor spreading rates for the past 3 Myr and slip directions over an

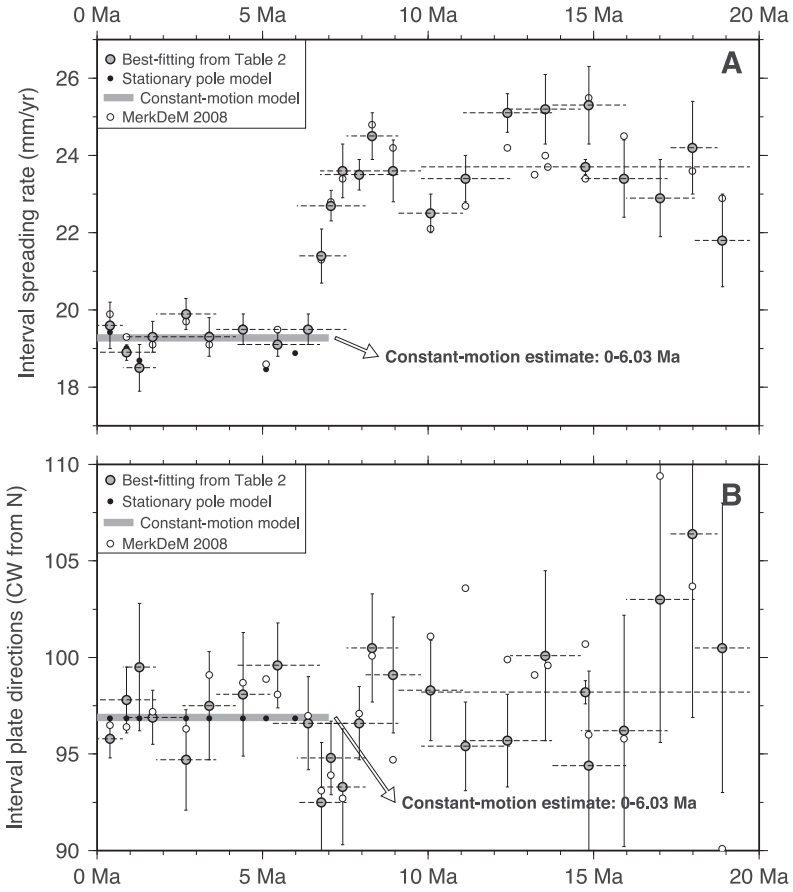

Figure 18. Estimates of interval plate rates (a) and directions (b) from Eurasia-North America stage rotations. Grey circles show best-fitting interval velocities that are derived from stage rotations that are determined from the plate motion rotations in Table 2. Black circles are estimated from the rotations that enforce a stationary pole from C3An.1 to the present (see text). Open circles are interval rates from Merkouriev & DeMets (2008). Grey bars show the rate and direction predicted by the best constant-motion model, consisting of a stationary pole and fixed angular rotation rate for the present back to C3An.1 (see text). Velocities are predicted at 59.2°N, 29.4°W along the Reykjanes Ridge. Velocity uncertainties are 95 per cent. Horizontal dashed lines specify the time interval that is spanned by a given stage rotation.

indeterminate time interval probably shorter than one million years (DeMets *et al.* 2010). Consequently, the Eurasia-North America plate velocities predicted by MORVEL should agree with velocities predicted by this study for times since ∼3 Myr. Figs 16 and 19 show that this is the case. The MORVEL Eurasia-North America pole (black star in Fig. 16) is located midway between the poles for C1no (0.78 Myr) and C2An.3 (3.60 Myr) and predicts opening rates and directions that differ by less than 0.7 mm yr^{-1} and 1° from the plate velocities estimated with our best-fitting rotations (e.g. Fig. 19). The MORVEL angular velocity and new rotation estimates are thus consistent.

6 CONCLUSIONS

More than 13 000 newly interpreted and previously published magnetic reversal, fracture zone and transform fault crossings for magnetic reversals C1 through C6no are used to quantify Eurasia-North America motion during the Quaternary and most of the Neogene periods. Inversions of more than 4000 crossings of reversals younger than 7 Ma from 16 geographically distinct, well-surveyed areas of the plate boundary give opening distance versus reversal age sequences that reveal average, two-sided outward displacement of magnetic polarity transition zones of 6 km along the magma-dominated Reykjanes Ridge and areas just north of the Charlie Gibbs fracture zone and 2 km elsewhere along the plate boundary. Rotations corrected for the outward displacement confirm the previously described 20 per cent slowdown in Eurasia-North America opening rates at 7.5–6.7 Ma (Merkouriev & DeMets 2008) and indicate that the pole of rotation shifted southward by ≈1000 km at the same time, farther than previously determined.

Systematic 5–20-km overrotations of magnetic lineations older than C5 along the Gakkel Ridge may be evidence for a previously unrecognized microplate or possible distributed deformation in the Arctic region before 10 Ma. The misfits imply that seafloor spreading rates across the Gakkel Ridge before 9.8 Ma were slower by ≈1 mm yr^{-1} than expected for Eurasia-North America motion in this region. The small spreading-rate deficit implies that any deformation or microplate movement was slow in relation to the motions of the major bounding plates.

The best-fitting Eurasia-North America rotations from Table 2 also systematically overrotate by 5–20 km anomalies older than C4A between the Azores triple junction and 42°N (Fig. 6). We speculate that distributed deformation or microplate deformation associated with the nearby Eurasia-North America-Nubia triple junction may have extended several hundred kilometres north of the present triple junction (39.6°N) before 7–8 Mybp. Additional work with the well-mapped magnetic fabric in this region (Luis & Miranda 2008) is needed to better understand deformation associated with the triple junction over the past 20 Myr.

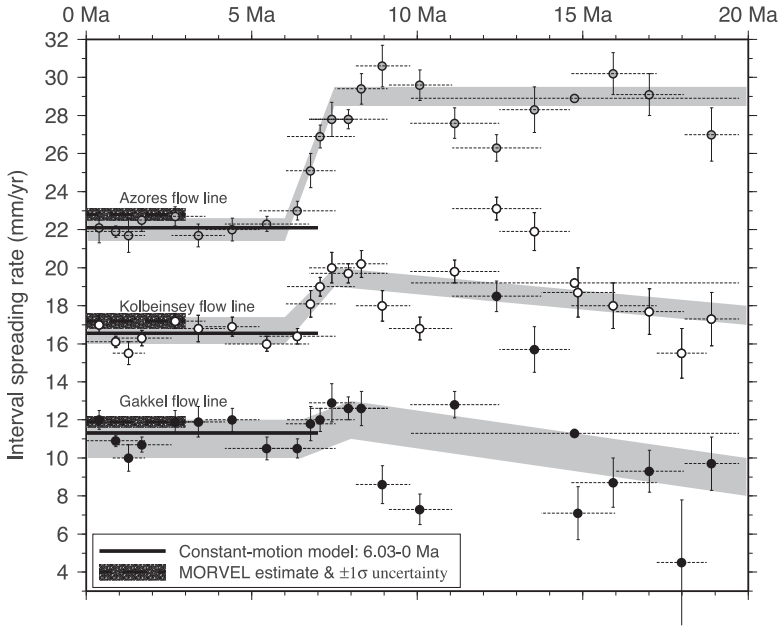

Figure 19. Interval seafloor spreading rates near the Azores triple junction, Kolbeinsey Ridge, and Gakkel Ridge predicted by Eurasia-North America stage rotations determined from the plate motion rotations of Table 2 (grey, white, and black circles, respectively). The bold solid and dashed lines show rates predicted by the constant motion model described in the text and the MORVEL Eurasia-North America angular velocity (DeMets *et al.* 2010), respectively. Azores, Kolbeinsey, and Gakkel interval rate histories are determined at 41.0°N 29.1°W, 69.5°N 16.0°W, and 85.6°N, 17.4°W, respectively. Horizontal dashed lines specify the time interval spanned by a given stage rotation. Uncertainties are 95 per cent. The grey-shaded areas approximate the interval rate histories for each flow line.

ACKNOWLEDGEMENTS

We thank Joaquim Luis for providing us with 1960s vintage Woods Hole Oceanographic Institute aeromagnetic data from north of the Azores triple junction and also thank two anonymous reviewers for constructive reviews of the manuscript. This work was supported by grant 06-05-64297 from the Russian Foundation for Basic Research and grant OCE-0926274 from the U.S. National Science Foundation. Figures were drafted using Generic Mapping Tools software (Wessel & Smith 1991).

REFERENCES

Atwater, T. & Mudie, J.D., 1973. Detailed near-bottom geophysical study of the Gorda Rise, *J. geophys. Res.,* **78,** 8665–8686.

Benediktsdóttir, A., Hey, R., Martinez, F. & Hoskuldsson, A., 2012. Detailed tectonic evolution of the Reykjanes Ridge during the past 15 Ma, *Geochem. Geophys. Geosyst.,* **13,** Q02008, doi:10.1029/2011GC003948.

Carbotte, S.M. *et al.*, 2004. New integrated data management system for Ridge2000 and MARGINS research, *EOS, Trans. Am. geophys. Un.,* **85,** 553–559.

Chang, T., 1988. Estimating the relative rotation of two tectonic plates from boundary crossings, *J. Am. Stat. Assoc.,* **83,** 1178–1183.

Crane, K., Doss, H., Vogt, P., Sundvor, E., Cherkashov, G., Poroshina, I. & Joseph, D., 2001. The role of the Spitsbergen shear zone in determining morphology, segmentation, and evolution of the Knipovich Ridge, *Mar. Geophys. Res.,* **22,** 153–205.

DeMets, C. & Wilson, D.S., 2008. Toward a minimum change model for recent plate motions: calibrating seafloor spreading rates for outward displacement, *Geophys. J. Int.,* **174,** 825–841.

DeMets, C., Gordon, R.G. & Argus, D.F., 2010. Geologically current plate motions, *Geophys. J. Int.,* **181,** 1–80.

Feden, R.H.R., Vogt, P. & Fleming, H., 1979. Magnetic and bathymetric evidence for the "Yermak Hot Spot" northwest of Svalbard in the Arctic Basin, *Earth planet. Sci. Lett.,* **44,** 18–38.

Fisher, N.I., Lewis, T. & Embleton, B.J.J., 1993. *Statistical Analysis of Spherical Data,* Cambridge Univ. Press, 329 pp.

Gaina, C., Roest, W.R. & Muller, R.D., 2002. Late Cretaceous-Cenozoic deformation of northeast Asia, *Earth planet. Sci. Lett.,* **197,** 273–286.

Géli, L., Renard, V. & Rommevaux, C., 1994. Ocean crust formation processes at very slow spreading centers: a model for the Mohns Ridge, near 72°N, based on magnetic, gravity, and seismic data, *J. geophys. Res.,* **99,** 2995–3013.

Glebovsky, V.Y., Kaminsky, V.D., Minakov, A.N., Merkuriev, S.A., Childers, V.A. & Brozena, J.M., 2006. Formation of the Eurasia Basin in the Arctic Ocean as inferred from geohistorical analysis of the anomalous magnetic field, *Geotectonics,* **40,** 263–281.

Gramkow, C., 2001. On averaging rotations, *J. Math. Imaging Vision,* **15,** 7–16.

Hellinger, S.J., 1979. The statistics of finite rotations in plate tectonics, unpublished *PhD thesis,* Massachusetts Institute of Technology, 172 pp.

Hellinger, S.J., 1981. The uncertainties of finite rotations in plate tectonics, *J. geophys. Res.,* **86,** 9312–9318.

Hey, R., Martinez, F., Hoskuldsson, A. & Benediktsdóttir, A., 2010. Propagating rift model for the V-shaped ridges south of Iceland, *Geochem. Geophys. Geosyst.,* **11,** Q03011, doi:10.1029/2009GGC002865.

Hilgen, F.J., Lourens, L. & Van Dam, J., 2012. The Neogene Period, in *The Geologic Time Scale 2012,* pp. 947–1002, eds Gradstein, F.M., Ogg, J.G., Schmitz, M. & Ogg, E.G., Elsevier.

Kovacs, L.C., Bernero, C., Johnson, G.L. Jr, Pilger, R.H., Taylor, P.T. & Vogt, P.R., 1982. *Residual Magnetic Anomaly Chart of the Arctic Ocean Region,* Naval Research Laboratory and Naval Ocean Research and Development Activity.

Lawver, L.A., Muller, R.D., Srivastava, S.P. & Roest, W., 1990. The opening of the Arctic Ocean, in *Geologic History of the Polar Oceans: Arctic Versus Antarctic,* pp. 29–62, eds Bleil, U. & Thiede, E J., Bremen, NATO Symposium, October, 1988.

Lourens, L., Hilgen, F.J., Laskar, J., Shackleton, N.J. & Wilson, D., 2004. The Neogene Period, in *A Geologic Time Scale 2004,* pp. 409–440, eds Gradstein, F., Ogg, J. & Smith, A., Cambridge Univ. Press.

Luis, J.F. & Miranda, J.M., 2008. Reevaluation of magnetic chrons in the North Atlantic between 35°N and 47°N: Implications for the formation

of the Azores Triple Junction and associated plateau, *J. geophys. Res.,* **113,** B10105, doi:10.1029/2008JB005573.

Macnab, R., Verhoef, J., Roest, W. & Arkani-Hamed, J., 1995. New database documents the magnetic character of the Arctic and North Atlantic, *EOS, Trans. Am. geophys. Un.,* **76,** 449–458.

Marques, F.O., Catalao, J.C., DeMets, C., Costa, A.C.G. & Hildebrand, A., 2013, GPS and tectonic evidence for a diffuse plate boundary at the Azores triple junction Earth planet. *Sci. Lett,* **381,** 177–187.

Merkouriev, S. & DeMets, C., 2006. Constraints on Indian plate motion since 20 Ma from dense Russian magnetic data: implications for Indian plate dynamics, *Geochem. Geophys. Geosyst.,* **7,** Q02002, doi:10.1029/2005GC001079.

Merkouriev, S. & DeMets, C., 2008. A high-resolution model for Eurasia-North America plate kinematics since 20 Ma, *Geophys. J. Int.,* **173,** 1064–1083.

Merkouriev, S. & DeMets, C., 2014. High-resolution estimates of Nubia-North America plate motion: 20 Ma to present, *Geophys. J. Int.,* **196**(3), 1281–1298.

Michael, P.J. *et al.*, 2003. Magmatic and amagmatic seafloor generation at the ultraslow-spreading Gakkel ridge, Arctic Ocean, *Nature,* **423,** 956–961.

Ogg, J.G., 2012. Geomagnetic polarity time scale, in *The Geologic Time Scale 2012,* pp. 85–113, eds Gradstein, F.M., Ogg, J.G., Schmitz, M. & Ogg, E.G., Elsevier.

Pitman, W.C. & Talwani, M., 1972. Sea floor spreading in the North Atlantic, *Bull. geol. Soc. Am.,* **83,** 619–646.

Rowley, D.B. & Lottes, A.L., 1988. Plate-kinematic reconstructions of the North Atlantic and Arctic: late Jurassic to present, *Tectonophysics,* **155,** 73–120.

Royer, J.-Y. & Chang, T., 1991. Evidence for relative motions between the Indian and Australian plates during the last 20 Myr from plate tectonic reconstructions: implications for the deformation of the Indo-Australian plate, *J. geophys. Res.,* **96,** 11 779–11 802.

Sandwell, D.T. & Smith, W.H.F., 1997. Marine gravity anomaly from Geosat and ERS 1 altimetry, *J. geophys. Res.,* **102,** 10 039–10 054.

Searle, R., 1981. The active part of Charlie-Gibbs Fracture Zone: a study using sonar and other geophysical techniques, *J. geophys. Res.,* **86,** 243–262.

Sempere, J.-C., Macdonald, K.C. & Miller, S.P., 1987. Detailed study of the Brunhes/Matuyama reversal boundary on the East Pacific Rise at 19°30′ S: implications for crustal emplacement processes at an ultra fast spreading center, *Mar. Geophys. Res.,* **9,** 1–23.

Sempere, J.-C., Kristjansson, L., Schouten, H., Heirtzler, J.R. & Johnson, G. L., 1990. A detailed magnetic study of the Reykjanes Ridge between 63°00′ N and 63°40′ N, *Mar. Geophys. Res.,* **12,** 215–234.

Seton, M. *et al.*, 2014. Community infrastructure and repository for marine magnetic identifications, *Geochem. Geophys. Geosyst.,* doi:10.1002/2013GC005176.

Shaw, P.R. & Cande, S.C., 1990. High-resolution inversion for South Atlantic plate kinematics using joint altimeter and magnetic anomaly data, *J. geophys. Res.,* **95,** 2625–2644.

Srivastava, S.P. & Tapscott, C.R., 1986. Plate kinematics of the North Atlantic Plate, in *The Western North Atlantic Region,* pp. 379–405, eds Vogt, P.R. & Tucholke, B.E., The Geology of North America M, Geol. Soc. Am.

Talwani, M. & Eldholm, O., 1977, Evolution of the Norwegian-Greenland Sea, *Geol. soc. Am. Bull.,* **88,** 969–999.

Verhoef, J., Roest, W., Macnab, R. & Arkani-Hamed, J. Members of the Project Team, 1996. Magnetic anomalies of the Arctic and North Atlantic Oceans and adjacent land areas, GSC Open File 3125, parts a and b (CD-ROM and project report), Geological Survey of Canada, Dartmouth, Nova Scotia, 225 pp.

Vogt, P.R., Taylor, P.T., Kovacs, L.C. & Johnson, G.L., 1979. Detailed aeromagnetic investigation of the Arctic Basin, *J. geophys. Res.,* **84,** 1071–1089.

Wessel, P. & Smith, W.H.F., 1991. Free software helps map and display data, *EOS, Trans. Am. geophys. Un.,* **72,** 441–446.

Wilson, D.S., 1993. Confidence intervals for motion and deformation of the Juan de Fuca plate, *J. geophys. Res.,* **98,** 16 053–16 071.